MITSUBISHI ELECTRIC RESEARCH LABORATORIES
https://www.merl.com

Safe and Constrained Rendezvous, Proximity Operations, and Docking

Petersen, Chris; Caverly, Ryan; Phillips, Sean; Weiss, Avishai

TR2024-016 March 12, 2024

Abstract

This tutorial paper discusses the rising need for safe and constrained spacecraft Rendezvous, Proximity Operations, and Docking (RPOD). This class of problems brings with it i) a unique set of equations of motion, ii) a variety of constraints and objectives that are specialized to RPOD, and iii) a number of traditional and current Guidance, Navigation, and Control (GNC) considerations. There are strong connections between the work done in RPOD and a variety of other research domains that have synergistically aided in pushing forward the state-of-the-art. This tutorial paper discusses the above, provides an entry point into the field of spacecraft RPOD, and highlights a selection of open problems that still exist in the field.

American Control Conference (ACC) 2023

Mitsubishi Electric Research Laboratories, Inc.
201 Broadway, Cambridge, Massachusetts 02139

Safe and Constrained Rendezvous, Proximity Operations, and Docking

Christopher Petersen*, Ryan J. Caverly†, Sean Phillips‡, and Avishai Weiss§

***Abstract*— This tutorial paper discusses the rising need for safe and constrained spacecraft Rendezvous, Proximity Operations, and Docking (RPOD). This class of problems brings with it i) a unique set of equations of motion, ii) a variety of constraints and objectives that are specialized to RPOD, and iii) a number of traditional and current Guidance, Navigation, and Control (GNC) considerations. There are strong connections between the work done in RPOD and a variety of other research domains that have synergistically aided in pushing forward the state-of-the-art. This tutorial paper discusses the above, provides an entry point into the field of spacecraft RPOD, and highlights a selection of open problems that still exist in the field.**

I. Introduction

Space is entering its second age, which, driven jointly by governmental and industrial demand signals [1], [2], is rapidly advancing spacecraft Rendezvous, Proximity Operations, and Docking (RPOD), which we define as any operation where two or more satellites are within 500 km. The interest in RPOD is exemplified by the amount of theoretical research over the years (see survey papers [3]–[6], and references therein), and the number of missions, beginning with the Apollo Program, continuing to International Space Station (ISS) docking [7], and more recently, to missions such as Prisma in 2010 by the Swedish Space Corporation [8], the Autonomous Nanosatellite Guardian for Evaluating Local Space (ANGELS) in 2014 by the United States Air Force (USAF), [9], Mycroft in 2018 by the USAF [10], the Mission Extension Vehicle (MEV) in 2019 by Northrup Grumman [11], the End-of-Life Services by Astroscale-demonstration (ELSA-d) in 2021 by Astroscale [12], and the planned on-orbit re-fueling with Starship by SpaceX [13]. Due to its relevance, RPOD technology has become an enabler for other missions such as satellite formation flight, modular spacecraft operations, and In-space Servicing, Manufacturing, and Assembly (ISAM) [14]–[16], all of which are complex and require strong safety guarantees. Thus, there is a need for Guidance, Navigation, and Control (GNC) algorithms that satisfy constraints, guarantee safety, and simultaneously achieve mission goals to the extent possible. This tutorial paper aims to introduce safe and constrained RPOD to a wide community, discusses current RPOD problems within the context of GNC, elaborates on constraints, presents the state-of-the-art in the field, and emphasizes connections to other research domains.

There have been several RPOD challenge and benchmark problems. The reference [17] presented an RPOD benchmark that ensured safety via hybrid automaton. The benchmark [18] enumerated the phases of the RPOD mission, including the available sensors and dynamics. In [19], a problem was formulated for close RPOD in both rotation and translation, while limiting the configuration of the satellite to a single thruster. A follow-on problem [20] listed relevant safety constraints, objectives, and metrics with multi-body, robotic RPOD. With the aim of developing advanced RPOD algorithms to alleviate the burden on satellite operators, [21] introduced discrete steps towards autonomous operation using the example of a docking maneuver. These challenge and benchmark problems provide an entry point into spacecraft RPOD research by deriving the equations of motion, listing a variety of constraints, and enumerating metrics by which to evaluate RPOD algorithms. The present tutorial paper follows a similar approach, with a focus on presenting unique challenges in the areas of GNC as it relates to RPOD safety.

In addition to presenting the RPOD problem, this tutorial highlights connections to techniques in other research communities, demonstrating how the state-of-the-art can be advanced by adjacent fields. We discuss open RPOD problems and research, where novel, non-traditional techniques will be needed.

The remainder of the paper is structured as follows. The notation used throughout the paper is introduced in Section II. In Section III, the mathematical model for RPOD problems is introduced, specifically for the context of two spacecraft orbiting the Earth. Emphasis is placed on the relative dynamics between these two satellites, relevant perturbation forces, and special cases that can be made to simplify the dynamics. Sections IV to VI focus on the areas of navigation, guidance, and control, mirroring a standard GNC loop, as shown in Fig. 1, where each section begins with basic objectives, followed by relevant constraints, and ending with case studies that highlight state-of-the-art techniques in those areas. Connections between RPOD and other research communities are presented in Section VII, followed by a discussion on open problems and ongoing RPOD research in Section VIII. Concluding remarks are provided in Section IX.

II. Preliminaries and Notation

$\mathbb{R}$, $\mathbb{R}^n$, $\mathbb{Z}$, and $\mathbb{Z}_{0+}$ are the sets of real numbers, the Euclidean space, integers, and non-negative integers, re-

Approved for public release; distribution is unlimited. Public Affairs approval number #AFRL-2023-0868.

*Assistant Professor, Department of Mechanical and Aerospace Engineering, University of Florida, Gainesville, FL 32611, c.petersen1@ufl.edu

†Assistant Professor, Department of Aerospace Engineering and Mechanics, University of Minnesota, Minneapolis, MN 55455, rcaverly@umn.edu

‡Research Mechanical Engineer, Air Force Research Laboratory - Space Vehicles Directorate, Kirtland AFB, Albuquerque, NM 87117

§Principal Research Scientist, Mitsubishi Electric Research Laboratories, Cambridge, MA 02139, weiss@merl.com

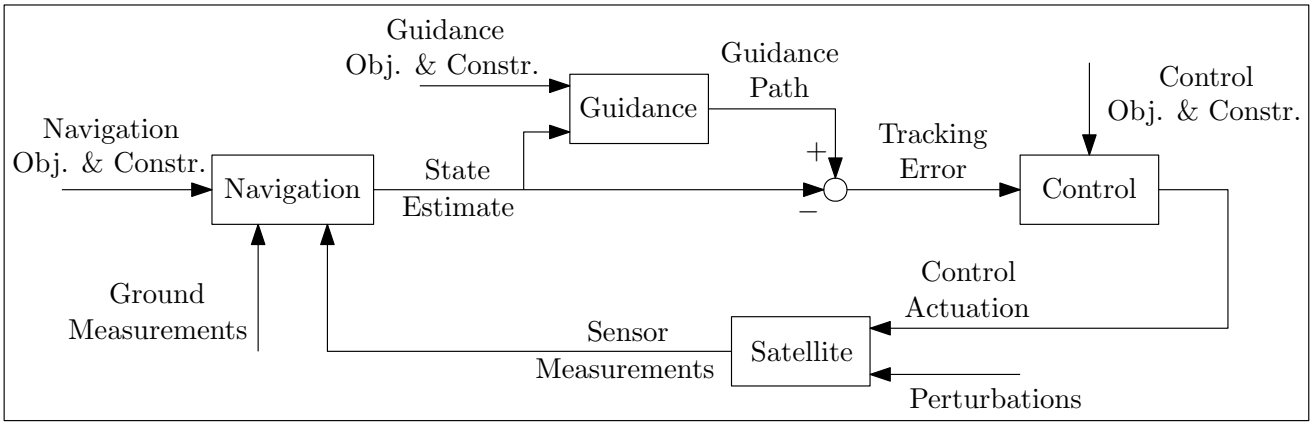

Fig. 1: A block diagram depicting the typical relationship between navigation, guidance, and control within the context of RPOD. Note that the abbreviation "Obj. & Constr." denotes "Objectives & Constraints."

spectively. Given a matrix $A \in \mathbb{R}^{n\times n}$, $\det(A)$ denotes its determinant and $\mathrm{tr}(A)$ denotes its trace. I_n denotes the n-dimensional identity matrix and 0_n denotes an $n \times n$ zero matrix. Given a vector $x \in \mathbb{R}^n$, the norm $||x||$ is the two norm $\sqrt{x^{\mathrm{T}}x}$ unless otherwise stated. Given vectors $y, z \in \mathbb{R}^3$, $[y]^\times : \mathbb{R}^3 \to \mathbb{R}^{3\times 3}$ is the skew symmetric operator such that $y \times z = [y]^\times z$.

A reference frame $\mathrm{F_X}$ is defined by a set of three orthonormal basis vectors $\{\hat{\imath}, \hat{\jmath}, \hat{k}\}$. The vector $\vec{r}_{\mathrm{q/p}}$ denotes the position of point q relative to point p, the vector $\vec{v}_{\mathrm{q/p/X}} = \overset{\mathrm{X}\cdot}{\vec{r}}_{\mathrm{q/p}}$ denotes the derivative of the position of point q relative to point p with respect to frame $\mathrm{F_X}$, and the vector $\vec{\omega}_{\mathrm{Y/X}}$ denotes the angular velocity of frame $\mathrm{F_Y}$ relative to frame $\mathrm{F_X}$. Note that $\vec{(\cdot)}$ denotes a coordinate-free (unresolved) vector, and $(\cdot)^{\mathrm{X}}$ denotes the vector resolved in frame $\mathrm{F_X}$. All frames are orthogonal and right-handed. The special orthogonal group is given as $\mathrm{SO}(3) = \{R \in \mathbb{R}^{3\times 3} : \det(R) = +1, R^\top R = I_3\}$. For additional discussion on physical vectors, frames, and notation, see [22], [23].

Given a continuous-time signal $x(t)$ sampled with period ΔT, we denote the value at time instant $k\Delta T$, $k \in \mathbb{Z}_{0+}$, by $x_k = x(k\Delta T)$, and $x_{j|k}$ denotes the value of x predicted j steps ahead from k. The hyperplane representation (H-representation) of the polyhedron $\mathcal{P} \subseteq \mathbb{R}^n$ is $\mathcal{P}(H, l) = \{x \in \mathbb{R}^n : \ Hx \leq l\}$ with $H \in \mathbb{R}^{p\times n}$, $l \in \mathbb{R}^p$. An ellipsoid centered at $d \in \mathbb{R}^n$ with shape matrix D is $\mathcal{E}(d, D) = \{x \in \mathbb{R}^n \ : \ (x-d)^\top D^{-1}(x-d) \leq 1\}$.

For brevity, it is assumed that unless otherwise stated, all constraints presented are to hold for all time.

III. Spacecraft RPOD Model

A. RPOD Equations of Motion

Consider the Earth Centered Inertial (ECI) frame $\mathrm{F_E}$ and an unforced particle e that is collocated with the center of the Earth (*Assumption 1*). Next, consider two spacecraft, an uncontrolled target and a controlled chaser, in orbit around the Earth[1]. The centers of mass of the target and chaser are denoted by t and c, respectively. The target and chaser are assumed to be rigid and all external forces are modeled as acting on their corresponding centers of mass (*Assumption 2*). The mass loss of the chaser spacecraft due to control is significantly smaller than the total mass of the spacecraft (*Assumption 3*). Under Assumptions 1-3, the translational equations of motion for the target and chaser relative to the inertial frame $\mathrm{F_E}$ are given by [24]

$$\begin{aligned} \overset{\mathrm{E}\cdot\cdot}{\vec{r}}_{\mathrm{t/e}} &= -\mu \frac{\vec{r}_{\mathrm{t/e}}}{||\vec{r}_{\mathrm{t/e}}||^3} + \frac{\vec{f}_{\mathrm{pt}}}{m_{\mathrm{t}}}, \\ \overset{\mathrm{E}\cdot\cdot}{\vec{r}}_{\mathrm{c/e}} &= -\mu \frac{\vec{r}_{\mathrm{c/e}}}{||\vec{r}_{\mathrm{c/e}}||^3} + \frac{\vec{f}_{\mathrm{pc}}}{m_{\mathrm{c}}} + \frac{\vec{f}_{\mathrm{c}}}{m_{\mathrm{c}}}, \end{aligned} \tag{1}$$

where $\vec{r}_{\{\mathrm{t,c}\}/\mathrm{e}}$ are the unresolved position vectors of the target and chaser center of mass relative to the center of Earth, μ is Earth's gravitational constant, $\vec{f}_{\mathrm{pt}}, \vec{f}_{\mathrm{pc}}$ are the vector sum of orbital perturbations on the target and chaser, $m_{\{\mathrm{t,c}\}} \in \mathbb{R}$ are the target and chaser masses, and $\vec{f}_{\mathrm{c}}$ is the controllable force vector applied to the chaser. For more precise modeling, certain assumptions may be relaxed, e.g., see [25] for models that include the effects of fuel slosh.

In RPOD, we are concerned with the motion of the chaser relative to the target in a relative orbit frame (often called Hill's frame), defined as $\mathrm{F_O} = \{\hat{\imath}_r, \hat{\imath}_\theta, \hat{\imath}_h\}$ with radial ($\hat{\imath}_r$), along-track ($\hat{\imath}_\theta$), and cross-track ($\hat{\imath}_h$) basis vectors. The vector $\hat{\imath}_r$ is parallel to the target position vector $r^{\mathrm{E}}_{\mathrm{t/e}} \in \mathbb{R}^3$, $\hat{\imath}_h$ points in the direction of the orbit's angular momentum, and $\hat{\imath}_\theta$ completes the frame [26], see Fig. 2.

The position of the chaser relative to the target is given by

$$\vec{r}_{\mathrm{c/t}} = \vec{r}_{\mathrm{c/e}} - \vec{r}_{\mathrm{t/e}}. \tag{2}$$

Taking the derivative of the relative position (2) with respect

[1]As a tutorial introduction to RPOD, we consider orbits around a central body. This can be expanded for other applications, see Section VIII for ongoing research on RPOD in cislunar space.

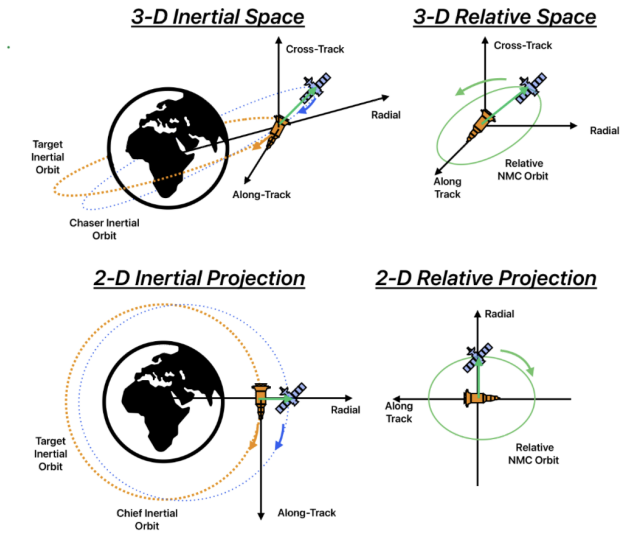

Fig. 2: Inertial (left) and relative motion (right) of the target and chaser in $\mathrm{F_E}$ (inertial space) and $\mathrm{F_O}$ (relative space).

to the target's orbital frame $\mathrm{F_O}$ yields the relative velocity

$$\overset{\mathrm{O}\cdot}{\vec{r}}_{\mathrm{c/t}} = \overset{\mathrm{E}\cdot}{\vec{r}}_{\mathrm{c/t}} - \vec{\omega}_{\mathrm{O/E}} \times \vec{r}_{\mathrm{c/t}}, \tag{3}$$

and the derivative of (3) with respect to the target's orbital frame $\mathrm{F_O}$ yields [26]

$$\begin{aligned}\overset{\mathrm{O}\cdot\cdot}{\vec{r}}_{\mathrm{c/t}} = \overset{\mathrm{E}\cdot\cdot}{\vec{r}}_{\mathrm{c/e}} - \overset{\mathrm{E}\cdot\cdot}{\vec{r}}_{\mathrm{t/e}} - \dot{\vec{\omega}}_{\mathrm{O/E}} \times \left(\vec{\omega}_{\mathrm{O/E}} \times \vec{r}_{\mathrm{c/t}}\right) \\ -2\vec{\omega}_{\mathrm{O/E}} \times \overset{\mathrm{E}\cdot}{\vec{r}}_{\mathrm{c/t}} - \overset{\mathrm{O}\cdot}{\vec{\omega}}_{\mathrm{O/E}} \times \vec{r}_{\mathrm{c/t}}.\end{aligned} \tag{4}$$

Substituting (1) into (4) results in the nonlinear relative equation of motion of the chaser with respect to the target. See [27] and [28] for an explicit presentation of these nonlinear relative equations resolved in the target's orbital frame $\mathrm{F_O}$.

For GNC design purposes and over short time horizons, the target can often be modeled to be in an unperturbed orbit, i.e., $\vec{f}_{\mathrm{pt}} = \vec{0}$ (*Assumption 4*). With the additional assumption that $\|\vec{r}_{\mathrm{c/t}}\| \ll \|\vec{r}_{\mathrm{t/e}}\|$ (*Assumption 5*), the relative dynamics in (1), (4) can be linearized and resolved in the target's orbital frame $\mathrm{F_O}$, resulting in [29]

$$\begin{aligned}\delta\ddot{x} - \left(\tfrac{2\mu}{r_{\mathrm{t}}^3} + \tfrac{h^2}{r_{\mathrm{t}}^4}\right)\delta x + \left(\tfrac{2\dot{\psi}}{r_{\mathrm{t}}^4}h\right)\delta y - \left(\tfrac{2\dot{h}}{r_{\mathrm{t}}^2}\right)\delta\dot{y} &= \tfrac{u_x+w_x}{m_{\mathrm{c}}}, \\ \delta\ddot{y} + \left(\tfrac{\mu}{r_{\mathrm{t}}^3} - \tfrac{h^2}{r_{\mathrm{t}}^4}\right)\delta y - \left(\tfrac{2\dot{\psi}}{r_{\mathrm{t}}^4}h\right)\delta x + \left(\tfrac{2\dot{h}}{r_{\mathrm{t}}^2}\right)\delta\dot{x} &= \tfrac{u_y+w_y}{m_{\mathrm{c}}}, \\ \delta\ddot{z} + \left(\tfrac{\mu}{r_{\mathrm{t}}^3}\right)\delta z &= \tfrac{u_z+w_z}{m_{\mathrm{c}}},\end{aligned} \tag{5}$$

where $r^{\mathrm{O}}_{\mathrm{c/t}} = \begin{bmatrix}\delta x & \delta y & \delta z\end{bmatrix}^{\mathsf{T}}$ is the relative position between the chaser and the target resolved in $\mathrm{F_O}$, $v^{\mathrm{O}}_{\mathrm{c/t/O}} = \begin{bmatrix}\delta\dot{x} & \delta\dot{y} & \delta\dot{z}\end{bmatrix}^{\mathsf{T}} \in \mathbb{R}^3$ is the relative velocity between the chaser and the target resolved in in $\mathrm{F_O}$, $r_{\mathrm{t}} = \|\vec{r}_{\mathrm{t/e}}\|$, $h = \left\|\vec{r}_{\mathrm{t/e}} \times \vec{v}_{\mathrm{t/e/E}}\right\|$ is the inertial specific angular momentum of the target's orbit, and $\psi = \vec{v}_{\mathrm{t/e/E}} \cdot \vec{r}_{\mathrm{t/e}}$. The term $u \triangleq f^{\mathrm{O}}_{\mathrm{c}} = \begin{bmatrix}u_x & u_y & u_z\end{bmatrix}^{\mathsf{T}} \in \mathbb{R}^3$ is the control input applied to the chaser resolved in $\mathrm{F_O}$, while $w \triangleq f^{\mathrm{O}}_{\mathrm{pc}} = \begin{bmatrix}w_x & w_y & w_z\end{bmatrix}^{\mathsf{T}} \in \mathbb{R}^3$ is the vector of perturbation forces acting on the chaser resolved in $\mathrm{F_O}$. Since for general orbits, r_{t} varies in magnitude along the orbit, (5) is a set of linear time-varying (LTV) equations that can be written compactly as

$$\dot{x}(t) = \tilde{A}(t)x(t) + \tilde{B}u(t) + \tilde{B}w(t), \tag{6}$$

where $x \triangleq \begin{bmatrix}r^{\mathrm{O}\mathsf{T}}_{\mathrm{c/t}} & v^{\mathrm{O}\mathsf{T}}_{\mathrm{c/t/O}}\end{bmatrix}^{\mathsf{T}} \in \mathbb{R}^6$.

The state solution of (6) is given by

$$x(t) = \Phi(t,t_0)x(t_0) + \int_{t_0}^{t} \Phi(t,\tau)\tilde{B}(\tau)\left(u(\tau)+w(\tau)\right)\mathrm{d}\tau, \tag{7}$$

where the state transition matrix (STM) $\Phi(t,t_0)$ is the solution to the initial value problem [30]

$$\begin{aligned}\dot{\Phi}(t,t_0) &= \tilde{A}(t)\Phi(t,t_0), \quad t \in [t_0,t], \\ \Phi(t_0,t_0) &= I_n.\end{aligned} \tag{8}$$

For implementation in digital computers, we often sample (6) with period ΔT small enough to not lose relevant inter-sampling behavior, obtaining

$$x_{k+1} = A_k x_k + B_k u_k + B_k w_k, \tag{9}$$

where A_k, B_k are the time-discretized matrices obtained based on the continuous-time system realization $(\tilde{A}, \tilde{B})$.

B. Circular Specialization of the Equations of Motion

Making use of Assumptions 4 and 5, and also considering the case in which r_{t} is constant[2] (*Assumption 6*), the equations in (5) reduce to the well known Hill-Clohessy-Wiltshire (HCW) equations [23]

$$\begin{aligned}\delta\ddot{x} - 3n^2\delta x - 2n\delta\dot{y} &= \frac{u_x+w_x}{m_{\mathrm{c}}}, \\ \delta\ddot{y} + 2n\delta\dot{x} &= \frac{u_y+w_y}{m_{\mathrm{c}}}, \\ \delta\ddot{z} + n^2\delta z &= \frac{u_z+w_z}{m_{\mathrm{c}}},\end{aligned} \tag{10}$$

where $n = \sqrt{\mu/r_{\mathrm{t}}^3}$ is the mean motion of the target's orbit. The HCW equations (10) are linear time-invariant (LTI) and can be compactly written as

$$\dot{x}(t) = \bar{A}x(t) + \bar{B}u(t) + \bar{B}w(t). \tag{11}$$

Similarly to the discrete-time LTV dynamics described in (9), the LTI dynamics of (11) can be discretized with a sampling period ΔT to obtain

$$x_{k+1} = Ax_k + Bu_k + Bw_k, \tag{12}$$

[2] 79% of all satellites in orbit are in a near circular orbit with eccentricity of < 0.025 (note that a perfect circular orbit has an eccentricity of $e = 0$) [31].

where A, B are the constant time-discretized matrices. Of particular note is A, which has a closed form solution

$$A = \begin{bmatrix} \Phi_{\mathrm{rr}}(\Delta T) & \Phi_{\mathrm{rv}}(\Delta T) \\ \Phi_{\mathrm{vr}}(\Delta T) & \Phi_{\mathrm{vv}}(\Delta T) \end{bmatrix}, \tag{13}$$

where

$$\begin{aligned} \Phi_{\mathrm{rr}}(t,t_0) &= \begin{bmatrix} 4-3p_c & 0 & 0 \\ 6(p_s-p) & 1 & 0 \\ 0 & 0 & p_c \end{bmatrix}, \\ \Phi_{\mathrm{rv}}(t,t_0) &= \tfrac{1}{n}\begin{bmatrix} p_s & 2(1-p_c) & 0 \\ 2(p_c-1) & 4p_s-3p & 0 \\ 0 & 0 & h_s \end{bmatrix}, \\ \Phi_{\mathrm{vr}}(t,t_0) &= n\begin{bmatrix} 3p_s & 0 & 0 \\ 6(p_c-1) & 0 & 0 \\ 0 & 0 & -p_s \end{bmatrix}, \\ \Phi_{\mathrm{vv}}(t,t_0) &= \begin{bmatrix} p_c & 2p_s & 0 \\ -2p_s & 4p_c-3 & 0 \\ 0 & 0 & h_c \end{bmatrix}, \end{aligned} \tag{14}$$

$p = n(\Delta T)$, $*_c = \cos(*)$, and $*_s = \sin(*)$ for the sake of brevity.

The sinusoidal functions in (14), which are the direct consequence of purely imaginary eigenvalues of A, result in closed "zero-fuel" trajectories known as natural motion circumnavigations (NMCs) [32]. Chaser spacecraft are often guided to NMCs, as they can remain arbitrarily close to the target for an indefinite period of time while consuming little fuel.

C. Translational Actuation Methods

The input $u(t)$ in (6) is generated by onboard mechanical actuation subsystems. These actuators have their own dynamics, limitations and safety constraints, which may need to be considered when designing RPOD solutions. For translational motion, actuation is normally produced by thrusters via chemical or electric reactions [33]–[35], each of which have advantages and disadvantages [36]. We give explicit definitions of these constraints in Section VI-A.

Chemical propulsion typically uses liquid or solid fuels that undergo a chemical reaction to generate thrust [33], [34]. The most common liquid fuels are liquid hydrogen, liquid oxygen, kerosene, or hydrazine, which react in a chamber to produce directional thrust. Chemical propulsion offers high thrust, which makes it a great candidate for the agile maneuvers needed in RPOD. Under this assumption of thrust, $u(t)$ is modeled as a unit impulse or dirac delta function. The limitation is that chemical thrusters use up fuel quickly, which restricts the capability of the satellite to perform routine maneuvers. Chemical thrusters are also not ideal for small and precise maneuvers due to their "on-off" actuation with imprecise, limited/slow duty cycle burns.

Electric Propulsion (EP) works by ionizing a propellant gas and then accelerating the resulting charged particles using electric fields in order to generate thrust [37]. There are several types of electrical propulsion systems including ion thrusters, Hall-effect thrusters, and plasma thrusters [33], [35], [37]–[39]. Due to the ionization, the particles can be accelerated to much higher speeds than in chemical thrusters, resulting in higher efficiency and lower propellant usage. EP systems can be continuously operated for long durations. As such, $u(t)$ can be modeled as a continuous signal or a zero-order-hold signal. Efficiency comes at a cost, however, as EP systems typically generate much less thrust than chemical propulsion systems, making them less suited for agile operations. Additionally, due to the ionization process, there are significant power requirements to operate EP systems, which requires additional solar arrays or other power sources. Finally, as the propulsion systems rely on electromagnetic fields to generate thrust, they can potentially interfere with other onboard electronics or nearby spacecraft.

In close proximity operations, regardless of the propulsion type, there is a risk of particles being expelled and interfering with another spacecraft. This interaction is expanded upon as a constraint in Section VI-A.2.

D. Perturbation Forces

Spacecraft are subject a host of non-Keplerian perturbations, represented by $w(t)$ in (6). Figure 3 depicts the perturbing accelerations $\frac{\vec{f}_{\mathrm{pt}}}{m_c}$ ($\frac{\vec{f}_{\mathrm{pc}}}{m_c}$) of various sources as a function of altitude. The main Keplerian gravitational

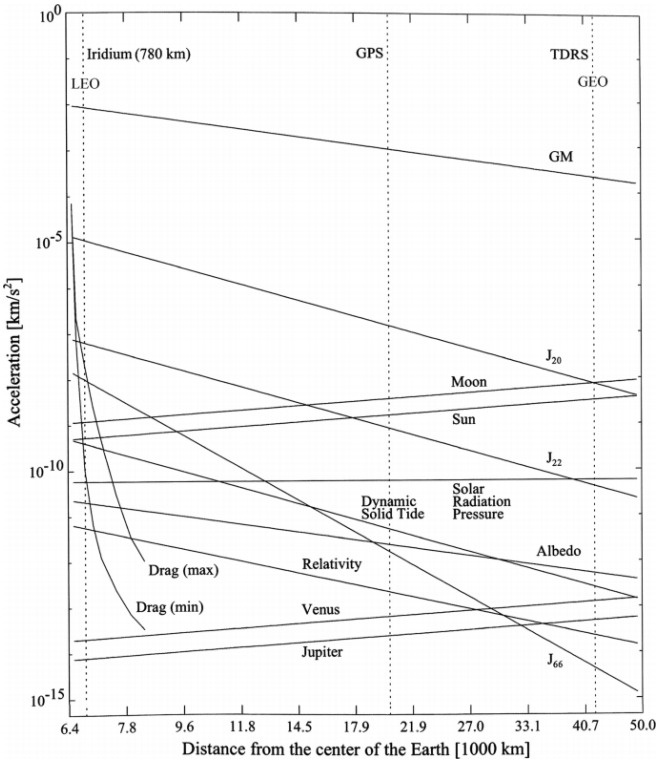

Fig. 3: Magnitude of orbital perturbation accelerations as a function of orbit altitude [24].

acceleration, denoted by GM in Fig. 3, has a magnitude on the order of $10 \times 10^{-2} - 10 \times 10^{-4}$ km/sec^2 and is

the dominant force acting on the satellite. This is explicit in (1) through the inverse-squared force terms. The next two dominant perturbations are the accelerations due to atmospheric drag and the higher-order gravitational terms due to fact that the Earth is not a perfect sphere. Details on these perturbations are provided as follows.

In Low Earth Orbit (LEO), atmospheric drag can be a significant source of perturbing acceleration. Very commonly, the magnitude of this perturbation is described by $||\vec{f}_{\mathrm{p,drag}}|| = \frac{1}{2}\rho_{\text{air}} v^2 C_d A$, where ρ_{air} is the atmospheric density, $v = \left\|\vec{v}_{\mathrm{c/e/E}}\right\|$ is the magnitude of the velocity of the satellite relative to the atmosphere, C_d is the satellite's drag coefficient, and A is satellite's projected frontal area. The direction of this perturbation force is in the opposite direction of the velocity of the satellite relative to the atmosphere, which can typically be approximated as acting in the direction opposite of the satellite's velocity relative to the center of the Earth with respect to frame $\mathrm{F_E}$ (e.g., in the opposite direction of $\vec{v}_{\mathrm{c/e/E}}$ for the chaser and similarly for the target). It is convenient to define the satellite's ballistic coefficient as $C_b = \frac{C_d A}{2m}$, which results in $||\vec{f}_{\mathrm{p,drag}}|| = m\rho_{\text{air}} v^2 C_b$. Note that the ballistic coefficient is sometimes defined as the reciprocal of this expression without the factor of one half. The expression used in this work is chosen to match [40], [41] out of convenience.

Another significant source of perturbation is due to the unequal mass distribution of the Earth, creating areas of complex gravity force. To match these effects, complex gravity perturbations are generally modeled using spherical harmonics [24]. Referencing Fig. 3, these effects are captured by $J_{a,b}$, where a, b are positive integers representing the particular harmonic. The most dominate harmonic, after GM is $J_{2,0}$ which is a consequence of how the Earth is shaped more like a elongated ellipsoid as opposed to a perfect sphere. While this is not as dominant in LEO, it becomes the second dominating perturbation at higher altitudes.

There are several other perturbations that can be considered as well, see [24]. It is ultimately the choice of the control engineer to determine which perturbations should be incorporated within the satellite model and which can be ignored at design and compensated for via feedback. This choice will depend on a number of factors, including the satellite's altitude, the time scale over which the satellite motion is being modeled, the geometry of the satellite, etc.

E. Attitude

While this tutorial paper is primarily focused on translational motion, it should be noted that the chaser and the target's rotation also have impacts on dynamics, guidance, navigation, and control. Generally in spacecraft RPOD, and similarly in other domains, rotational equations of motion are decoupled from the translational equations of motion. This is due in part to the scale of actuation; attitude actuation happens on the order of seconds to minutes whereas translational relative motion most commonly (though not always) occurs on the order of several minutes, to hours, or even days when not in close proximity. To model rotation, assume there is a body-fixed frame $\mathrm{F_B}$ in addition to the orbital frame $\mathrm{F_O}$ and the ECI frame $\mathrm{F_E}$. The rotational kinematics and dynamics are given by [42]

$$\dot{\mathcal{O}}_{\mathrm{B/E}} = -[\omega^{\mathrm{B}}_{\mathrm{B/E}}]^{\times} \mathcal{O}_{\mathrm{B/E}}, \tag{15}$$

$$J\dot{\omega}^{\mathrm{B}}_{\mathrm{B/E}} = -[\omega^{\mathrm{B}}_{\mathrm{B/E}}]^{\times} J\omega^{\mathrm{B}}_{\mathrm{B/E}} + \tau^{\mathrm{B}}, \tag{16}$$

where $\mathcal{O}_{\mathrm{B/E}} \in SO(3)$ is the direction cosine matrix that transforms a vector expressed in $\mathrm{F_E}$ to $\mathrm{F_B}$ (or equivalently describes the orientation of $\mathrm{F_B}$ relative to $\mathrm{F_E}$), J is the inertia matrix of the spacecraft relative to its center of mass and resolved in $\mathrm{F_B}$, and τ^{B} are the external torques acting on the satellite resolved in $\mathrm{F_B}$. It should be noted that while the rotational kinematics are expressed in terms of direction cosine matrices, there are other representations of attitude that can be used, such as Euler Angles, quaternions, Modified Rodrigues Parameters (MRPs), to name a few [43]. Each of these attitude representations have their own advantages and disadvantages, as discussed in [43], [44].

The rotational equations above are not specialized to spacecraft, in fact, they apply to any vehicle with rotational equations of motion. There are some interesting aspects to rotational dynamics, however, within the context of spacecraft. For example, a spacecraft often has principal inertia values that are significantly different, creating large nonlinear couplings in (16). While these nonlinearites can create complexities in some missions, they have been exploited in others, an example of which is the Kepler space telescope [45]. There is also a uniqueness to the manner in which actuation is applied to the rotational dynamics of spacecraft. The torques in (16) can either be produced with external moments (e.g., via thrusters or magnetorquers) or internal actuation (e.g., via reaction wheels or control moment gyroscopes). See [46] for a discussion on these actuation methods.

In the context of RPOD, there are circumstances in which it may be necessary to consider coupling between translational and rotational dynamics. For example, when treating non-center-of-mass points on the target and chaser spacecraft, e.g. docking ports, a kinematic coupling is established [47], [48]. Spacecraft translation and rotation can also exhibit dynamic coupling, e.g., through actuator placement [49], [50] as often spacecraft thrusters aren't aligned to provide pure forces and pure torques. If a satellite has dedicated actuators for translation and dedicated actuators for rotation, then this coupling can vanish due to a control steering law [51]. However, for spacecraft that have fewer degrees of freedom in control [19], or if some of the thrusters are favored over others, then rotation may be necessary to align the thrusters in the desired direction. There are also several constraints that could be due to thruster placement, one of which is emission, which is discussed further in Section VI-A.2.

Another source of dynamic rotational-translational coupling occurs when considering higher-fidelity disturbance forces in the equations of motion, such as the inclusion of atmospheric drag. As discussed in Section III-D, the drag force acting on the spacecraft is a function of its

projected frontal area and drag coefficient, which together can be combined into the spacecraft's ballistic coefficient, and typically vary with the spacecraft's attitude. This results in an attitude-dependent perturbation force that may have a noticeable effect on the spacecraft's motion, depending on the altitude and the time-scale considered.

F. Case Study: Drag Utilization

In addition to being a disturbance, drag can be leveraged for actuation, provided that the frontal area or drag coefficient of the satellite can be adjusted. It is convenient to summarize both frontal area and drag coefficient modification as modulation of the satellite's ballistic coefficient. Examples of actuation devices designed specifically for the modulation of a satellite's ballistic coefficient include the Exo-Brake [52], which is a sail-like drag device that can be modulated using a winch system, and the D3 device [53], which uses deployable booms to change the spacecraft's frontal area.

These devices provide the possibility of adjusting the satellite's ballistic coefficient, which can then be thought of as a control input. The magnitude of control accelerations that are achievable by this source of actuation are generally small in magnitude, but have the benefit of not requiring any fuel. Examples of applications that make use of drag for actuation include satellite formation keeping [54], targeted re-entry [52], [54]–[57], and constellation phasing [58], [59]. For simplicity in this tutorial paper, actuation using drag is limited to a single satellite whose goal is to track a target orbit. In this case, the target satellite can be thought of as a "virtual" target whose dynamics are governed by the satellite with its nominal ballistic coefficient C_b. The chaser satellite is then representative of the actual satellite, which has a ballistic coefficient of $C_b+\Delta C_b$, where ΔC_b represents the controllable change in ballistic coefficient. The relative equations of motion are then derived by substituting the differential drag force

$$f^{\mathrm{O}}_{\mathrm{pc,drag}} - f^{\mathrm{O}}_{\mathrm{pt,drag}} \approx \begin{bmatrix} 0 \\ 0 \\ -m\rho_{\mathrm{air}}v^2 \end{bmatrix} \Delta C_b \qquad (17)$$

into (1) and (4). The resulting relative equations of motion can be linearized about the trajectory of the spacecraft with ballistic coefficient C_b, which yields LTV equations of the form in (6), where ΔC_b is considered as a control input [41].

There are challenges associated with using ballistic coefficient modulation as a form of actuation. One of these challenges is that the magnitude of the resulting drag force depends on the atmospheric density, which is not accurately known in practice and will change as a function of altitude, longitude, latitude, time of day, space weather, etc. This makes it difficult to predict the drag forces produced by a change in ballistic coefficient. It has been shown in [60] that space weather forecasts and atmospheric density models, such as the NRLMSISE-00 model [61], can be used to predict atmospheric density conditions along the satellite's trajectory within a predictive control framework and that Kalman filtering techniques can be used to correct for inaccuracies in this prediction using measurements of satellite position and velocity. Another challenging aspect of this control approach is that the satellite is underactuated when relying solely on ballistic coefficient modulation, as the control input only acts in the along-track direction. Dynamic coupling between the along-track and radial directions can be leveraged in the design of the controller, as done in [41], however, the cross-track dynamics remain uncontrollable. This can be addressed by either simply accepting drift in this direction or augmenting ballistic coefficient modulation with an additional source of actuation. Moreover, there are strict limits on the range of ΔC_b that is achievable as a control input. This places strict input constraints on any control strategy that is implemented, which has been accounted for using an Model Predictive Control (MPC)-based control strategy in [41]. An example of the trajectory tracking capabilities of the MPC approach in [41] compared to the Linear Quadratic Regulator (LQR) in [40] is provided in Fig. 4. It is worth noting that the MPC formulation in [41] assumes the satellite's rotational and translational dynamics are decoupled, which can be achieved in practice through either an inner-loop attitude controller or a drag device that is designed to passively stabilize the satellite to point in the direction of its velocity vector. The MPC approach used for ballistic coefficient modulation in [41] is further elaborated on in Section VI-C.

IV. Navigation

The objective of RPOD navigation is to compute the chaser's inertial orbit (i.e., $\overrightarrow{r}_{\mathrm{c/e}}$ and $\overrightarrow{v}_{\mathrm{c/e/E}}$) and its relative orbit to the target (i.e., the state x in (6) or (11)) reliably and safely. In order to do this, a number of onboard and on-the-ground sensors can used, giving rise to two classes of navigation constraints; those that ensure sensor safety, and those that ensure filter safety. These are explained below, with an introduction section on satellite measurement sources.

A. Satellite Measurement Sources

Traditionally there are two ways to obtain the inertial position and velocity of the chaser, either via an infrequent transmission from the ground or frequent transmission from GPS. In both cases, the variance in this measurement is generally a function of the distance from the center of the Earth. For satellites in LEO, ground measurements and GPS can give an accurate inertial position and velocity. For satellites in Geostationary Orbit (GEO), measurements are less accurate, as triangulation is difficult due the GPS satellites being in an orbit of lower altitude. As such, these types of measurements alone may not be sufficient to achieve the accuracy needed for RPOD.

Measurements for relative motion are generally obtained from onboard cameras that operate either in the visible or the infrared spectrum. A simple measurement is called "angles-only," which consists of two relative angles between the chaser and target (this is also called bearings only in

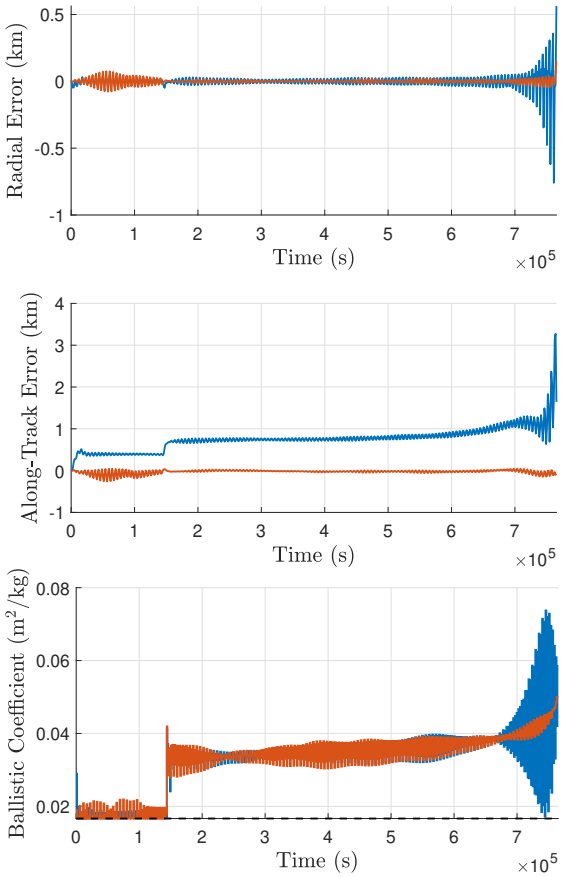

Fig. 4: Results of tracking a target re-entry trajectory from LEO using modulation of the satellite's ballistic coefficient as the control input. The results in red utilize the LQR controller from [40] with only knowledge of the satellite's current state, while the red results utilizes the MPC approach of [41] and a forecast of the atmospheric density. The dashed line represents the ballistic coefficient's lower limit, which is explicitly enforced as an input constraint within the MPC approach. When using the LQR controller, the ballistic coefficient is simply saturated when commanded outside of its feasible range.

some domains). Typically this type of measurement scheme can be performed all the way to the outer boundary of RPOD (e.g., a relative distance of 500 km). While simple, there exists a lack of observability in range for angles-only, as multiple angles and angular rates give rise to the same NMCs [62]. In the literature, there are two schools of thought to combat this range ambiguity. The first is to add more realism into the model used by the navigation filter through more complex dynamics [63]. This induces a weak observability at the cost of computational complexity. A second option is to thrust at diverse parts of the orbit (not just perigee or apogee) in order to increase the quality of measurements [64]. Though not a hard constraint on the system, such a requirement on desired maneuver diversity can be achieved using methods like dual-control, where the objective to obtain diverse measurements is included in the cost function to minimize. Further details on this approach are discussed in the case study of Section IV-E.

More recently, satellite technology has advanced to the point where computer vision can assist in navigation [65], [66]. Since computer vision relies on identifying key features, it is able to provide an accurate relative position measurement without the range ambiguity, albeit, at the cost of more computation and additional constraints, and is discussed further in Section IV-C.

B. Sensor Safety Constraints

While in RPOD ranges, it is best practice to have "eyes-on" the target so that the chaser receives constant measurements for use in its navigation filter. This artificially imposes an assumption that the chaser always has a camera sensor pointing at the target This also constrains the chaser to ensure that no bright objects are in-line with the chaser and target, which is important for two main reasons. First, is to ensure the physical camera hardware is not damaged. Second, if there is a bright object in the field-of-view that does not harm the sensor (e.g., the Earth), the navigation filter might lose track of the target, which will violate the objective of reliable navigation. This creates a keep-out cone constraint that can be mathematically transcribed as

$$\frac{\vec{r}_{\mathrm{c/t}} \cdot \hat{b}}{||\vec{r}_{\mathrm{c/t}}||} \leq \cos(\theta_{min}), \tag{18}$$

where the exclusion boresight unit vector and angle are defined as $\hat{b}$ and θ_{min}, respectively. The three major boresight exclusion vectors commonly used are in the directions of the Sun, Earth, and Moon [67].

C. Filter Safety Constraint

When considering the reliably of a navigation filter, a prime constraint is the angular velocity of the chaser relative to the target. If the chaser is rotating too fast, then it is difficult to obtain a good image and process it quickly. In the worst-case scenario, the target, which ideally would appear as a dot in the field of view, would appear as a streak, providing false measurements. It is ideal to limit the relative angular velocity, which can be transcribed into the following constraint

$$\left|\left| \frac{\overset{\mathrm{O}\cdot}{\vec{r}}_{\mathrm{c/t}}}{||\vec{r}_{\mathrm{c/t}}||} - \frac{\overset{O\cdot}{\vec{r}}_{\mathrm{c/t}} \cdot \vec{r}_{\mathrm{c/t}}}{||\vec{r}_{\mathrm{c/t}}||^2} \right|\right| \leq \nu_{max}, \tag{19}$$

where ν_{max} is the maximum angular rate the satellite can move about the target.

For computer vision, key points or features need to be visible to the camera, which in some instances provide a unique constraint when performing RPOD. This is because, as the chaser satellite approaches the target satellite, there is the possibility of "self-shadowing," in which case the chaser casts a shadow on the target, thereby eclipsing several key points or features necessary for RPOD. The major factor in this is the direction of the Sun, but in contrast to the previous

angles-only constraint that was formulated to restrict bright objects from being behind the target, this also restricts a bright object from being behind the chaser. One way to formulate this constraint is via a docking corridor (which can be a guidance constraint), which can be cast as an inclusion cone constraint

$$\frac{\overrightarrow{r}_{\mathrm{c/t}} \cdot \hat{b}_{\mathrm{dock}}}{||\overrightarrow{r}_{\mathrm{c/t}}||} \geq \cos(\theta_{\mathrm{dock}}), \tag{20}$$

where $\hat{b}_{\mathrm{dock}}$ and θ_{dock} represent a unit vector from the bright object to the chaser and its inclusion angle, respectively.

D. Metrics of Navigation Performance and Efficiency

Navigation performance and efficiency metrics are typically concerned with a) how quickly does the navigation solution converge to the true state and b) what is the bound on the navigation error, whether it be from a hard upper/lower bound perspective or a stochastic perspective. From a classical systems theory standpoint, one metric that can reflect the quality of measurements over a given time t is norm of the observably Gramian [30], given by

$$\int_0^t \left|\left|\Phi(\tau,t_0)^{\mathsf{T}} H(\tau)^{\mathsf{T}} H(\tau)\Phi(\tau,t_0)d\tau\right|\right|, \tag{21}$$

where H is the observability matrix and $\Phi(t,t_0)$ is the STM defined in (8). Another metric that can be used is the integration of the trace of the state covariance matrix L over time, given by

$$\int_0^t ||\mathrm{tr}(L(\tau))d\tau||, \tag{22}$$

which is commonly used in aspects of dual control [68] and covariance control [69]. When taking this metric into account when maneuvering, the chaser may deviate from efficient trajectories and NMCs to get diverse measurements, as discussed in the next case study.

E. Case Study: Observably Concerned RPOD with Angles-Only Measurements

One methodology to improve range-ambiguity of angles-only measurements is optimizing over two different metrics of performance: one relating to state-error and one relating to estimation variance. Often these metrics are optimized by combining the two in the same cost function. This lends itself to the following optimization problem.

$$\begin{aligned}\min_{\mathcal{U}} \quad & \sum_{k=0}^{N-1} \left(\hat{x}_{k|t}^{\mathsf{T}} Q \hat{x}_{k|t} + u_{k|t}^{\mathsf{T}} R u_{k|t} + \alpha \mathrm{tr}(L_{k|t})\right) \\ & + \hat{x}_{N|t}^{\mathsf{T}} Q_f \hat{x}_{N|t} + \alpha_f \mathrm{tr}(L_{N|t}) \end{aligned} \tag{23}$$

subject to

$$\hat{x}_{k|t} = F_1(x_{k|t}, u_{k|t}, y_{k|t}), \tag{24}$$

$$L_{k|t} = F_2(x_{k|t}, u_{k|t}, y_{k|t}), \tag{25}$$

$$x_{k+1|t} = A\hat{x}_{k|t} + Bu_{k|t}, \tag{26}$$

$$u_{min} \leq u_{k|t} \leq u_{min}, \tag{27}$$

where $\mathcal{U}$ is the set of admissible control inputs; $Q = Q^{\mathsf{T}} \geq 0$, $R = R^{\mathsf{T}} > 0$, and $Q_f = Q_f^{\mathsf{T}} > 0$ are weighting matrices on state-error, control, and terminal error; F_1, F_2 are the filtering dynamics, commonly produced by a Kalman filter or an Extended Kalman Filter (EKF); $\hat{x}$ is the mean state; $L = L^{\mathsf{T}} > 0$ is the variance produced by the Kalman filter; the discrete-time LTI dynamics in (26) correspond to the dynamics in (12); and $\alpha, \alpha_f > 0$ are tuning parameters that can be chosen to put emphasis on either control or navigation. It should be noted that the filter dynamics also have process noise associated with them, in order to ensure that the filter "does not go to sleep" [70].

Such an optimization will tend to balance two conflicting objectives. On one hand, the optimizer will try to minimize the state error and fuel to stabilize at a desired goal, e.g., reach and maintain zero relative position and velocity, which in turn necessitates that the fuel consumption be close to zero. On the other hand, in order to gain information, the satellite may need to move to obtain diverse measurements, which necessitates constant fuel consumption to achieve a property known as persistent excitation [71]. Balancing these two objectives can be done using the α, α_f parameters in (23).

This framework can be used in RPOD, where the navigation inputs considered in this case study are from angles-only navigation, with preliminary results shown in Fig. 5. The results depict two control-estimation methodologies; The first method is an LQR control with an EKF, represented by dashed-lines. The second is using the dual-control method in (23)-(27) represented by solid line. The top plot in Fig. 5 demonstrates that the dual-control method takes a longer route, but the trace of the covariance in the bottom plot of Fig. 5 remains closer to zero. The closer the trace is to 0, the more confident the chaser is in its estimate. Thus the dual-controller takes a non-intuitive path in order to gain more information than the LQR controller, but at the cost of fuel. It should also be noted that the dual-control method also strictly enforces upper and lower bound control constraints, guaranteeing safety during the operation.

V. Guidance

The objective of RPOD guidance is to generate a path that meets desired objectives while enforcing safety constraints. An important distinction for RPOD guidance is that the term "path" refers to both position space and velocity space, as an orbit needs both position and velocity to be defined. In terms of RPOD specific goals, most often it is required that at the end of the path the chaser reaches the target (such as for docking) or an area around the target (such as a NMC). This section will address several path constraints, some of which are common in various research domains, and some of which are specialized to the space domain.

A. Position Safety Constraints

1) Keep-Out Zones: As the chaser performs proximity operations around the target, there may be physical locations where the chaser may not travel, e.g., locations with drifting

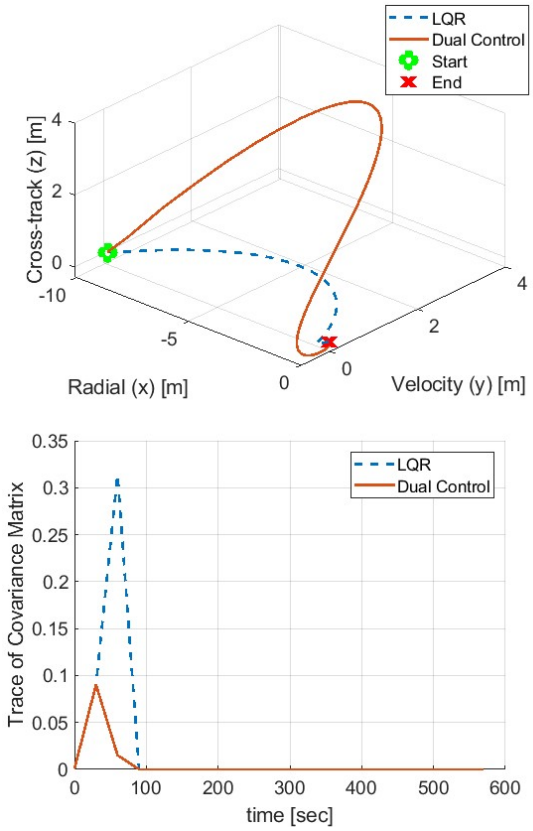

Fig. 5: Results of observability maneuvering for angle-only navigation. Dashed lines is using LQR feedback results with an EKF. Solid line shows dual control results with EKF.

debris or other obstacles. While there are multiple ways to express geometric vehicle shapes and constraints, one of the most common and computationally tractable ways is via ellipsoids, so that mathematically the chaser is outside an ellipsoid (and thus safe), if

$$1 \leq (r^{\mathrm{O}}_{\mathrm{c/t}} - r^{\mathrm{O}}_{\mathrm{o/t}})^{\mathsf{T}} P (r^{\mathrm{O}}_{\mathrm{c/t}} - r^{\mathrm{O}}_{\mathrm{o/t}}), \tag{28}$$

where P is the shape matrix of an ellipsoid and $r^{\mathrm{O}}_{\mathrm{o/t}}$ is the position vector of the center of the keep out zone. This constraint is non-convex, and often is handled via convexification or over-conservatism [72], [73]. Within close proximity, it may be desired to model the chaser and target as a collection of shapes, though often this is more computationally complex [74].

An extension of the keep-out zone constraint is the passive safety constraint. In this context, passive safety requires that if, in mid-operation, the thrusters are turned off, the chaser will drift and not collide with other objects. One formulation of this constraint leverages (7). Assuming the thrusters actuate N times at instances $t_j,\ j = 1, ..., N$, the jth passive safety constraint can be written as

$$1 \leq (\bar{r}_j(t) - r^{\mathrm{O}}_{\mathrm{o/t}})^{\mathsf{T}} P (\bar{r}_j(t) - r^{\mathrm{O}}_{\mathrm{o/t}}), \quad \forall t \in [t_0, t_c] \tag{29}$$

where

$$\bar{r}_j(t) = \begin{bmatrix} I_3 & 0_3 \end{bmatrix} \left(\Phi(t, t_0) x(t_0) + \int_{t_0}^{t_j} \Phi(t, \tau) \tilde{B}(\tau) u(\tau) \mathrm{d}\tau \right), \tag{30}$$

and t_c is the safety horizon for which the passive safety constraint is to be enforced. An alternative representation is described in the case study in Section V-C.

2) Velocity Safety Constraints: As with a majority of vehicles, there are often absolute limits on how quickly a spacecraft can travel. The velocity safety constraint is given by

$$\left\| \overset{\mathrm{O}\cdot}{\vec{r}}_{\mathrm{c/t}} \right\| \leq v_{max}, \tag{31}$$

where $v_{max} > 0$ is the absolute velocity constraint, which can be handled in most applications as it is a simple, convex constraint.

A unique velocity constraint is called range-rate, which intuitively creates a bound on velocity depending on the range between satellites. When the chaser is far away, there is little risk in colliding with the target and the rate at which they are approaching is of little immediate concern. In contrast, if the chaser is close to the target, the slower the chaser will want to proceed to preserve safety. This can be mathematically transcribed as a constraint on the velocity pointing towards the chaser

$$-\frac{\vec{r}_{\mathrm{c/t}} \cdot \overset{\mathrm{O}\cdot}{\vec{r}}_{\mathrm{c/t}}}{||\vec{r}_{\mathrm{c/t}}||^2} \leq k_{rr}, \tag{32}$$

where k_{rr} is a constant value chosen by the operator. The larger the value of k_{rr}, the more risk is taken by the chaser quickly approaching the target, and thus more risk to the vechicle.

B. Metrics of Guidance Performance and Efficiency

In spacecraft RPOD guidance, there are a couple of considerations to account for: a) how long does the trajectory take and b) how much effort does the trajectory take. The time metric $t_f = t - t_0$ has strong ties to minimum time optimization [75]. This metric also has connections with the period of the orbit and can be alternatively cast as $\frac{n}{2\pi} t_f$, where n is the orbital mean motion. While in an optimization setting minimizing the two metrics is equivalent, often RPOD missions are to be completed within a certain number of orbits, for which the second metric is more natural to use in the problem formulation.

The total fuel consumed is the metric associated with how much effort is required to perform the trajectory and is described by

$$\int_0^{t_f} ||u(\tau)|| d\tau. \tag{33}$$

The amount of fuel consumed is often strongly correlated with the thruster configuration and actuation laws, which are discussed within the context of control metrics in Section VI-B.

C. Case Study: Passive and Active Abort Safety

If the chaser suffers a severe software or hardware fault, the chaser will power off its thrusters and drift. To minimize collision risk, it is required that the chaser does not enter a restricted region, or keep-out zone, around the target while drifting, requiring passive safety. In close proximity to the target, particularly on a docking approach in which a controlled soft collision between the chaser and the target is required, an entirely passive approach may not be feasible. In such a scenario *active safety* is required, where, in the event of a fault, the chaser must be able to perform a *powered-abort maneuver* with its available thrust to avoid colliding with the target. Guidance and control techniques for active and passive safety may be found in [76]–[78], and references therein.

A recent approach to satisfying the active and passive safety requirements is to characterize the abort-unsafe regions of the state space using backwards reachable sets of an exclusion region $\mathcal{S}$ around the target with respect to the admissible after-failure input set $\mathcal{U}$ through the LTV dynamics (9) [78], [79]. The exclusion region may be represented by a polytope $\mathcal{P}$ or an ellipsoid $\mathcal{E}$. The backwards reachable sets determine the conditions from which the chaser will *necessarily* reach the exclusion region around the target regardless of the controls applied with the available thrust, and hence the initial states in the unsafe region from which collision cannot be avoided. Note that passive safety is the specialization of the after-failure admissible input set $\mathcal{U}$ to be the zero-input singleton $\{0\}$. Such backwards reachable sets are the union of convex sets for different initial and final times along the target's orbit, and hence are usually non-convex [80]. By maintaining the chaser state outside of the unsafe region, there is always a control sequence that avoids collision in the presence of faults. As above in Section V-A.1, avoiding the backwards reachable sets is a non-convex constraint. To obtain a problem that can be solved in real-time, the constraint is convexified by constructing linear constraints that locally separate the chaser from the backwards reachable sets. An MPC policy is developed to enforce the local constraints, yielding abort-safe rendezvous trajectories that evolve in the region in which safe passive or active aborts are guaranteed to exist. Fig. 6 shows the results of the MPC policy that does (6b) and does not (6a) enforce passive safety constraints. The free-drift trajectories along the nominal unsafe rendezvous maneuver intersect the exclusion region, while the MPC policy that enforces the passive safety constraint yields free-drift trajectories that do not enter the exclusion zone. Fig. 6c shows a simulation of an MPC policy that does and does not enforce active safety constraints prior to a fault in which only a single thruster remains functional. The unsafe controller cannot avoid entering the exclusion region, while the safe controller can. An extension of this work to handle navigation and control uncertainty was developed in [81], and an extension to the case of rendezvous on a near rectilinear halo orbit about the Moon was developed in [79].

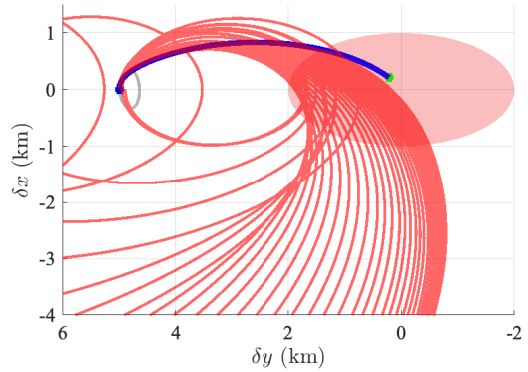

(a) *Passively unsafe rendezvous* for a target in an eccentric orbit. States along the trajectory enter the exclusion zone under free-drift dynamics.

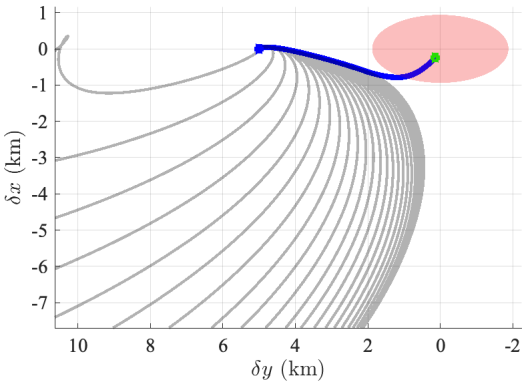

(b) *Passively safe rendezvous* for a target in an eccentric orbit. States do not enter the exclusion zone within the safety horizon under free-drift dynamics.

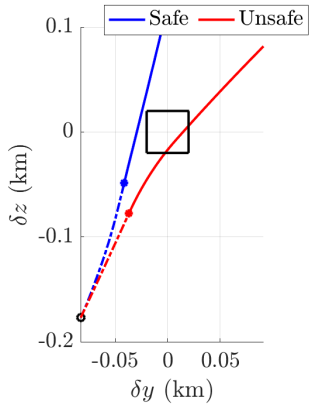

(c) *Actively safe rendezvous*, comparison of safe and unsafe controllers when a single thruster remains available after fault. Dashed and solid lines are states before and after propulsion failure, respectively.

Fig. 6: Abort-Safe Rendezvous. The trajectory of the relative position of the chaser with respect to the target as seen in the target's orbital frame $\mathrm{F_O}$ is shown for passive safety in (a),(b) and for active safety in (c).

VI. Control

The objective of RPOD control is like many other research areas: how precisely can a guidance path be tracked? This

often assumes that a path is given as a time series of waypoints that need to be followed by some controller. This may even entail understanding what specific thrusters to use (e.g., the control allocation problem). It should be noted that for some applications, guidance and control loops can be combined, in which case the following safety metrics can be rolled into the same problem, but whether combined or not, the constraints below reflect necessary considerations when dealing with spacecraft thrusters.

A. Safety Constraints

1) Thrust Constraints: Fuel is a very limited resource on orbit and must be conserved. One way to do this is through the thrust constraint

$$||u|| \in [u_{min},\ u_{max}], \tag{34}$$

where $u_{min}, u_{max} > 0$. The maximum thrust constraint intuitively relates to the need to save fuel, and thrusters also have physical limits. The minimum fuel limit is necessary for two reasons. Firstly, satellite thrusters can be coarse and as such can only execute commands within a certain thrust magnitude. Secondly, and more subtly, although constant smaller thrusts may be effective in driving down tracking error, they can lead to accumulated fuel usage quite quickly. Thus, the minimum thrust constraint allows for a small amount of tracking error to build up before being corrected by a thrust maneuver, which can ultimately help save fuel [67].

In addition to the thrust constraint (34), total fuel of a maneuver can also be constrained as

$$\int_0^{t_f} ||u(\tau)||d\tau \leq u_{total}, \tag{35}$$

where u_{total} relates to the upper bound on maneuver fuel consumption. Limiting the total fuel enables more propellant to be used in the long term, increasing the life and utility of the chaser.

2) Thruster Particulate Emissions Mitigation: As the chaser performs proximity operations and docking, the direction of thrust becomes important. As described in Section III-C, the thruster of the chaser should not be directly aimed at the target when in close proximity. More specifically, the shape of the thruster emissions is characterized pre-launch, which typically resembles a conical region around the thrust vector with angle α centered at the bore-sight of the thruster. Let N_c be the number of thrusters on the chaser, u_{c_i} be the control input of the i-th thruster on the chaser, and α_{c_i} be the angle of the i-th thruster, where $i \in \{1, \ldots, N_c\}$. Thrusters also have a distance where the density of particulates is so low that the potential for interaction is negligible, which is denoted by $\gamma_{c_i} > 0$. More specifically, the thruster particulate emissions constraint can be written as

$$\cos^{-1}\left(\frac{u_{c_i}^{\mathsf{T}} r_{\mathrm{c/t}}^{\mathrm{O}}}{||r_{\mathrm{c/t}}^{\mathrm{O}}||}\right) \leq \frac{\alpha_{c_i}}{2}$$

for each $i \in \{1, \ldots, N_c\}$ if the i-th thruster is active and the chaser is in close enough relative proximity to the target.

B. Metrics of Control Performance and Efficiency

Control metrics for RPOD include the fuel efficiency metric (33), as well as several others that relate to specific thruster directions. One of these relates to the maximum fuel consumption across all of the thrusters. Sometimes this relates to a particular thruster configuration, but for simplicity we can examine the thrust in a body-fixed frame $\mathrm{F_B}$. Let $\mathcal{O}_{\mathrm{B/E}}$ be the direction cosine matrix that describes the orientation of $\mathrm{F_B}$ relative to $\mathrm{F_E}$. Then, in this frame the metric can be expressed using the infinity norm as

$$||\mathcal{O}_{\mathrm{B/E}} u||_\infty. \tag{36}$$

Another good metric to observe is actuation in individual body-fixed directions. This can be used to ensure that the thrusters are being used equally which can then improve mission lifetime. Such a metric can be expressed as

$$||\mathcal{O}_{\mathrm{B/E}} u||_1, \tag{37}$$

which is a one norm constraint.

As an interesting note, the type of norm chosen for (34) can be related to the thruster configuration on satellite. Typically, when a 2-norm is used, this relates to measuring the sum use of control across all the thrusters as one (i.e., considering the total thrust as if it were produced by a single thruster), whereas the use of a 1-norm relates to measuring the maximum fuel usage across all individual thrusters.

C. Case Study: Station Keeping via MPC

MPC is a receding-horizon combined guidance and control strategy that exploits a model of the system dynamics in order to determine a set of control inputs and a trajectory that minimizes a cost function, while satisfying state and control constraints over a finite future prediction horizon [82]. There are a number of MPC variations that can be implemented, including linear, nonlinear, robust, and adaptive MPC formulations, just to name a few [83]. One of the simplest implementations is linear quadratic MPC, which involves LTI system dynamics, a quadratic cost function, and affine constraints on the states and control inputs. With a discrete-time model, this leads to the optimization problem

$$\min_{\mathcal{U}} \ \sum_{k=0}^{N-1} \left(x_{k|t}^{\mathsf{T}} Q x_{k|t} + u_{k|t}^{\mathsf{T}} R u_{k|t}\right) + x_{N|t}^{\mathsf{T}} Q_f x_{N|t} \tag{38}$$

subject to

$$x_{k+1|t} = A x_{k|t} + B u_{k|t} + B w_{k|t}, \tag{39}$$

$$x_{min} \leq x_{k|t} \leq x_{max}, \tag{40}$$

$$u_{min} \leq u_{k|t} \leq u_{min}, \tag{41}$$

where N is the prediction horizon; $\mathcal{U} = \{u_{0|t}, \ldots, u_{N-1|t}\}$ is the sequence of control inputs over the prediction horizon; (38) is the quadratic cost function defined by $Q = Q^{\mathsf{T}} \geq 0$, $R = R^{\mathsf{T}} > 0$, and $Q_f = Q_f^{\mathsf{T}} \geq 0$ is often chosen as the solution to the algebraic Riccati equation; (39) represents the system's LTI dynamics in discrete time found in (12), where $w_{k|t}$, $k = 0, \ldots, N-1$ is a sequence of known

disturbances over the prediction horizon starting at time t; and the constraints to be maintained on the states and control inputs over the prediction horizon are specified by (40) and (41), respectively. A convenience of linear quadratic MPC is that it can be solved as a quadratic problem, which facilitates its use in real-time applications.

Satellites in GEO require regular station keeping maneuvers to maintain their latitude and longitude in the presence of perturbation forces that are dominated by the gravitational pull of nearby bodies (e.g., the Sun, the Moon, other planets), Earth's non-spherical shape (i.e., higher-order spherical harmonic gravitational terms), and solar radiation pressure. Although the individual station keeping thrusts are small in magnitude, they can add up to a significant amount of fuel over the entire satellite lifetime. Nominally, the GEO satellite is to maintain a circular orbit and thus, the motion of the satellite relative to this orbit can be described in a relative frame through the LTI relative dynamics of (12), where w contains all the relevant perturbation forces. This application can be related to RPOD by thinking of the nominal orbit as the virtual target and the satellite as the chaser. Station keeping requirements are often specified in terms of a "window" in the relative frame, where the satellite is deemed to be sufficiently close to the desired orbit. This can be specified as a constraint on the allowable relative position in the along-track and cross-track directions through $|\delta y| \leq \delta y_{max}$, $|\delta z| \leq \delta z_{max}$, where δy_{max} and δz_{max} are the maximum allowable deviations in the along-track and cross-track directions. In the case of GEO station keeping, the maximum deviations are described by $\delta y_{max} = r_t \tan(\lambda_{long})$ and $\delta z_{max} = r_t \tan(\lambda_{lat})$, where r_t is the GEO radius and the angles λ_{long} and λ_{lat} are maximum allowable deviations in longitude and latitude, respectively. One of the benefits of defining a station keeping window requirement is that the satellite is allowed to drift within this window, which limits the need to constantly correct for deviations from the nominal GEO position and velocity.

Linear quadratic MPC is well-suited to handle autonomous station keeping, as the relative dynamics in (12) are LTI, station keeping window constraint can be formulated as a state constraint, and thrust magnitude limits can be included as control input constraints. Moreover, an estimate of the expected perturbation forces acting on the satellite over an interval of future time is known, which allows for them to be incorporated into the MPC formulation. This procedure is outlined for a GEO station keeping application in [50], where the goal is to minimize fuel, while enforcing station keeping window constraints and using electric thrusters with relatively small thrust magnitude capabilities. Knowledge of the predicted future disturbances allows for efficient drifting of the satellite within the station keeping window (as shown in Fig. 7), resulting in relatively low fuel consumption.

The versatility of MPC in station keeping applications was demonstrated in [84], where a very similar formulation to [50] was used to perform aerostationary Mars orbit station keeping. Interestingly, the study in [84] illustrated the potential to further minimize station keeping fuel by pursuing a nonlinear MPC formulation. This involved using the full nonlinear equations of motion to better capture nonlinear coupling between the perturbation forces and the system's dynamics. Returning to the drag utilization scheme described in Section III-F, MPC is a practical solution for many of the same reasons given for station keeping. In this case, state constraints are of less concern, whereas input constraints on the allowable change in ballistic coefficient are critical. Aside from this, the main challenge of implementing MPC for drag utilization is incorporating a suitable estimate of the atmospheric density. As shown in [41], the discrepancy between the nominal density (e.g., the density predicted using space weather forecasts and an atmospheric model) and the actual local density can be accounted for by an additive input disturbance to the relative dynamics. Estimates of this disturbance can be obtained through past satellite trajectory data and on-board measurements [60], [85], which are then used as known disturbances within the MPC optimization scheme.

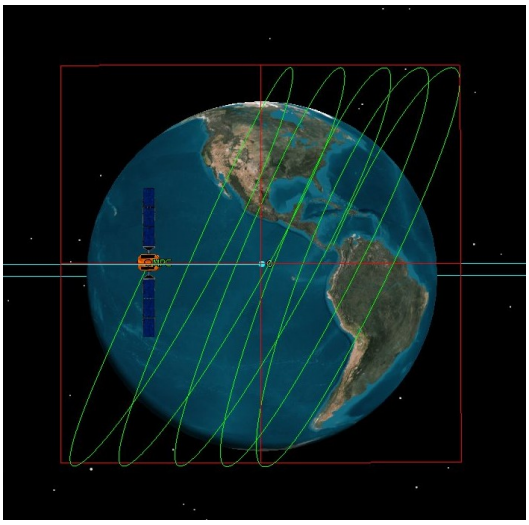

Fig. 7: Example of a GEO station keeping simulation, where MPC is used to minimize the fuel needed to meet the station keeping window constraint (red) by allowing for drift within the station keeping window. In this image, the along-track (East) direction is to the right, the cross-track direction (North) is upwards, and the radial direction is out of the page. The green trail shows the satellite position over the last five orbits.

D. Case Study: Underactuated Satellite Docking Control

There may be several reasons that a satellite is left without use of its full control capabilities. For example, [86] outlines a control methodology for reestablishing full actuation through the Hubble telescope's two reaction wheel failures, or [87] for recovering the Kepler telescope through similar methods. Moreover, there may be limited actuation due to an intentional design choice to lower the amount of spatial requirements for actuation hardware. This was the case in [19], where a satellite had only a single axial thruster by design, yet had a reaction wheel so it could

rotate as needed. Thus, for the specialized case of planar translational motion (i.e., the first two equations of (10)) with a single thruster, the satellite has two actuators for 3 degrees of freedom, resulting in an underactuated system. As the rotation is only about a single axis, the rotational dynamics become

$$I_c\ddot{\theta} = -I_w u_w, \tag{42}$$

where u_w is the control input into the reaction wheel, I_c and I_w are the moments of inertia of the chaser satellite and the reaction wheel, respectively. The planar translational dynamics with the single thruster then become

$$\begin{aligned} \delta\ddot{x} - 3n^2\delta x - 2n\delta\dot{y} &= \frac{u_T\cos(\theta) + w_x}{m_c}, \\ \delta\ddot{y} + 2n\delta\dot{x} &= \frac{u_T\sin(\theta) + w_y}{m_c}, \end{aligned} \tag{43}$$

where u_T is the control input for the single thruster. Note that the control matrix B is dependent on the orientation of the axial thruster, and more specifically, the assumption of uncoupled rotational and translational dynamics no longer applies. The specific problem becomes then to design a control algorithm to converge the state of the chaser satellite to the origin with $(\theta, \dot{\theta}) = (0, 0)$.

There are inherent issues with this problem that result in many common control design tools being unavailable. Specifically, [88] outlined several structural issues. Firstly, the linearized dynamics of the spacecraft system about the origin via a Taylor series expansion approximation is neither controllable nor stabilizable. Secondly, there exists no coordinate transformation that transforms the nonlinear dynamics into a locally controllable linear system about the origin. Thirdly, there exists no coordinate transformation and static state feedback for the spacecraft system that allows the closed-loop dynamics to become feedback linearizable into a locally controllable system about the origin. Finally, the so-called free system[3] is not, in general, Lyapunov stable. More in-depth discussion maybe found in [88]. It is possible, however, to show that any small angle around the origin is both controllable and stabilizable, which leads to the intuition that stability of the origin can be proven for this system. It is worth noting that the above dynamics are similar to the dynamics of a nonholonomic vehicle with an additional drift term representing the underlying natural relative motion between satellites. To solve this problem, theoretical tools from geometric control were leveraged; see [90], [91] for more information.

Through a Lie Algebra approach, a switching controller was designed that stabilized subsets of the state components to the origin, while holding others Lyapunov stable [88]. Recognizing that switching between these two stabilizing controllers can be performed in an intelligent manner, stability to the origin can be realized. Figure 8 shows the case of 100 numerical simulation initialized with a uniform distribution of initial conditions, see [88] for more information.

[3]The free system is Lyapunov stable when initialized in a closed natural trajectory, see [89].

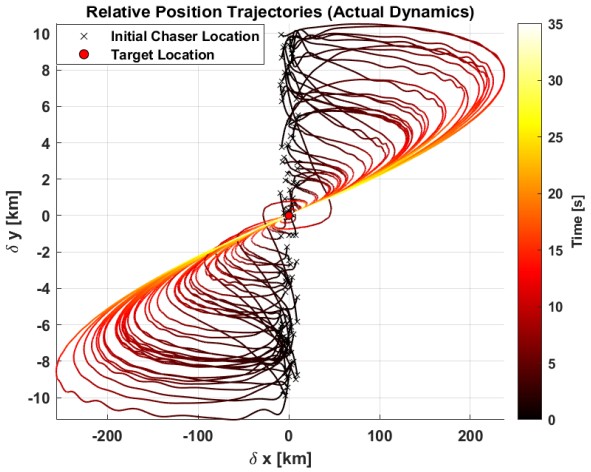

Fig. 8: One hundred numerical solutions of the switching control algorithm driving the underactuated chaser satellite to the docking configuration.

Nonlinear MPC, which is a formulation similar to (38) and (39) with the discrete-time dynamics constraint of (39) instead given by nonlinear equations $x_{k+1|t} = f(x_{k|t}, u_{k|t})$ where the mapping $f : \mathbb{R}^n \times \mathbb{R}^m \to \mathbb{R}^n$ maybe contain nonlinear instances of $x_{k|t}$ and $u_{k|t}$, may also be leveraged, as in [92], which is capable of incorporating input constraints, state safety constraints and final position/orientation, but is difficult and time consuming to compute.

VII. Connections Between RPOD and Other Research Applications

GNC research in RPOD has a strong historical connection to other research applications. Strides in RPOD leverage advances in other domains and vice versa, creating a feedback loop that advances the overall state-of-the-art.

From a navigational perspective, angles-only navigation using pixel measurements is common in spacecraft [93], [94] and Unmanned Aerial Vehicles (UAVs) [95], [96]. When closer to the target, pose estimation using computer vision [65], [66], [97] has strong connections to computer science and robotics [98], [99]. Furthermore, all RPOD navigation necessitates reliable filtering in relatively unknown, and sometimes GPS limited, environments, similar to UAVs [100], [101] and underwater vehicles [102], [103].

From a guidance perspective, the goal of calculating a path under stringent computational limitations is common across many vehicles, from small UAVs to autonomous driving. RPOD techniques that leverage closed-form guidance solutions like artificial potential functions [104], [105] are frequently used for UAVs and autonomous driving [106], [107]. On-board optimization techniques utilizing graph searches with positively invariant sets [108]–[110] leverage parallel efforts in the general guidance community [111], [112], and as one specific example, for lane change and

parking motion planning in the automotive regime [113]–[117]. Furthermore, recent advances in convex programming and convexification techniques have dominated the field of real-time optimization, not just space, in recent years [118], [119].

From the control perspective, RPOD thruster allocation uses linear and quadratic programs, which are widely used in general optimization applications [120]. In addition, RPOD typically involves control loops and signals that update at asynchronous rates [121], [122], which has close ties to hybrid dynamical systems tools and applications [123]–[125].

These are only a few of the many highlights of RPOD technology and their connections to other domains. Commonalities between these different application areas has allowed for the transfer of knowledge and techniques, which in part has helped the RPOD community expand greatly over the past several years.

VIII. Open Problems and Ongoing Research

In this tutorial, we have formalized a significant portion of the GNC challenges and solutions regarding safe and constrained RPOD. However, there are still a variety of open questions in the field, from general unanswered problems in the RPOD regime to exciting new challenges in on-orbit autonomy algorithms, logistics, and cislunar missions. A great challenge is moving from integrated operator control, towards onboard mission oriented autonomy.

Firstly, one of the large topics of interest on the horizon is in-space logistics. In-terms of on-orbit servicing, the state-of-the-art is reflected by Northrup Grumman with their Mission Extension Vehicle (MEV) in 2021 [11]. Upcoming missions by DARPA [126] and NASA [127] are designed to demonstrate and test the state of the art in multi-body satellite control. Logistics also includes the objective of space debris removal, which has become of interest with demonstrations, such as Astro-Scale's ELSA-D [128]. These types of logistics problems have many unique objectives, key among them: the need to compensate for contact mechanics when docking; develop guidance and control methods that can accommodate vehicles with long, possibly multi-body mechanical devices; and address the GNC challenges that arise when two spacecraft bodies come into contact to form as a single rigid body.

Secondly, there is great interest in the cislunar regime, given NASA's Artemis program and a variety of other countries launching in the next several years. While spacecraft missions are planned to be situational assets initially, there will come a need soon to manage, track, control, and decommission, as is now the case with the Earth. While there are a number of lessons learned that can be transitioned from Earth-centered RPOD, there are new complexities to be considered. With the cislunar domain, the dynamics are nonlinear, chaotic, and assumptions that are often made to obtain simple relative dynamics are no longer applicable. In addition, while RPOD in halo orbits has gained interest in the last several years [79], [129]–[132], these halo orbit evolve on time scales and distances far different than Earth-centered orbits. There are advantages in exploiting the chaotic relative dynamics, but there are still open challenges in navigation in this cislunar regime, as there is no GPS availability and communication options are sparse [133], [134]. From a control perspective, station keeping becomes challenging, as the chaotic dynamics result in less-intuitive strategies outside of the standard "thrust at perigee and apogee."

Finally, there are still challenges that exist for general Earth-centered RPOD. As spacecraft RPOD missions extend from a "target and chaser" to "one target and multiple deputies," more safety constraints manifest themselves. To enable such coordination of multiple deputies orchestrating their movements, there are numerous challenges. From a safety perspective, the number of safety constraints increases with the number of deputies, which affects the computational requirements of all spacecraft involved. As the number of deputies increases, the challenges of communication over dynamic networked graphs also becomes an issue. From a guidance and control perspective, this leads to challenges in multi-obstacle avoidance, as well as rapidly evolving constraints between vehicles. From a navigation perspective, there are questions as to how measurements should be fused to create accurate estimates, e.g. multiperspective pose estimation, and how it can be ensured that filters do not fail when multiple satellites are within the field of view. In addition, there are still open questions regarding how to make satellites more resilient to unknown and rapidly changing environments. With the solar cycle staring to enter a period of rise towards solar maximum, the likelihood of solar event-caused malfunctions increases. Recently such a case was attributed to SpaceX losing a large number of Starlink satellites due to a geomagnetic storm coinciding with their launch [135]. Ensuring that satellites remain safe, even in these drastic and unknown situations, is needed.

IX. Conclusion

This paper provided an entry point to the area of safe and constrained RPOD. The unique challenges associated with RPOD from dynamics, navigation, guidance, and control perspectives were presented in a tutorial manner, along with examples of GNC techniques that are being developed to address these challenges. A substantial number of open problems remain in the area of safe and constrained RPOD, which can benefit from collaborative efforts between members of the space research community and the broader GNC community. The hope is that this tutorial paper serves as a catalyst for further collaboration between these communities to enable great advances in RPOD capabilities.

References

[1] *U.S. Department of Commerce Strategic Plan — 2022 – 2026*. U.S. Department of Commerce, 2022.

[2] *United States Space Priorities Framework*. U.S. White House, 2022.

[3] C. Zagaris, M. Baldwin, C. Jewison, and C. Petersen, "Survey of spacecraft rendezvous and proximity guidance algorithms for onboard implementation," *25th AAS/AIAA Space Flight Mechanics Meeting*, 2015.

[4] D. Scharf, F. Hadaegh, and S. Ploen, "A survey of spacecraft formation flying guidance and control (part I): Guidance," in *American Control Conference*, 2003, pp. 1733–1739.

[5] ——, "A survey of spacecraft formation flying guidance and control (part II): Control," in *American Control Conference*, 2004, pp. 2976–2985.

[6] B. J. Naasz and M. C. Moreau, "Autonomous RPOD technology challenges for the coming decade," in *AAS Guidance, Navigation and Control Conference*, 2012.

[7] J. L. Goodman, "History of space shuttle rendezvous and proximity operations," *Journal of Spacecraft and Rockets*, vol. 43, no. 5, pp. 944–959, 2006.

[8] "Prisma's Tango and Mango satellites," https://www.esa.int/ESA_Multimedia/Images/2010/10/Prisma_s_Tango_and_Mango_satellites".

[9] "Air Force ANGELS: Satellite escorts to take flight," https://www.space.com/1816-air-force-angels-satellite-escorts-flight.html.

[10] "Mycroft - satellite space experiment," https://afresearchlab.com/technology/space-vehicles/mycroft/.

[11] "Mission Extension Vehicles succeed as Northrop Grumman works on future servicing/debris clean-up craft," https://www.nasaspaceflight.com/2021/05/mev-success-ng-future-servicing/.

[12] "Astroscale celebrates successful launch of ELSA-d," https://astroscale.com/astroscale-celebrates-successful-launch-of-elsa-d/.

[13] E. Seedhouse, *SpaceX: Starship to Mars–The First 20 Years*. Cham, Switzerland: Springer, 2022.

[14] X. Zhihui, L. Jinguo, W. Chenchen, and T. Yuchuang, "Review of in-space assembly technologies," *Chinese Journal of Aeronautics*, vol. 34, no. 11, pp. 21–47, 2021.

[15] M. A. Post, X.-T. Yan, and P. Letier, "Modularity for the future in space robotics: A review," *Acta Astronautica*, vol. 189, pp. 530–547, 2021.

[16] M. Luu and D. E. Hastings, "Review of on-orbit servicing considerations for low-earth orbit constellations," *ASCEND*, p. 4207, 2021.

[17] N. Chan and S. Mitra, "Verifying safety of an autonomous spacecraft rendezvous mission," in *ARCH17. 4th International Workshop on Applied Verification of Continuous and Hybrid Systems*, ser. EPiC Series in Computing, G. Frehse and M. Althoff, Eds., vol. 48, 2017.

[18] C. Jewison and R. S. Erwin, "A spacecraft benchmark problem for hybrid control and estimation," in *IEEE Conference on Decision and Control*, 2016, pp. 3300–3305.

[19] C. Petersen, S. Phillips, K. Hobbs, and K. Lang, "Challenge problem: Assured satellite proximity operations," *31st AAS/AIAA Space Flight Mechanics Meeting*, 2021.

[20] C. Petersen, "Challenge problem: Close proximity operations for spacecraft in-space servicing, manufacturing, and assembly," in *AAS/AIAA Spaceflight Mechanics Meeting 2023*, 2023, pp. AAS 23–387.

[21] K. L. Hobbs, J. B. Lyons, M. S. Feather, B. P. Bycroft, S. Phillips, M. Simon, M. Harter, K. Costello, Y. Gawdiak, and S. Paine, "Space trusted autonomy readiness levels," in *IEEE Aerospace Conference*, 2023.

[22] P. C. Hughes, *Spacecraft Attitude Dynamics*, 2nd ed. Mineola, New York: Dover, 2004.

[23] A. H. J. de Ruiter, C. J. Damaren, and J. R. Forbes, *Spacecraft Dynamics and Control: An Introduction*. West Sussex, UK: John Wiley & Sons, Ltd., 2013.

[24] O. Montenbruck, E. Gill, and F. Lutze, "Satellite orbits: Models, methods, and applications," *Applied Mechanics Reviews*, vol. 55, no. 2, pp. B27–B28, 2002.

[25] P. Gasbarri, M. Sabatini, and A. Pisculli, "Dynamic modelling and stability parametric analysis of a flexible spacecraft with fuel slosh," *Acta Astronautica*, vol. 127, pp. 141–159, 2016.

[26] J. L. Junkins and H. Schaub, *Analytical Mechanics of Space Systems*. AIAA, 2009.

[27] K. T. Alfriend, S. R. Vadali, P. Gurfil, J. P. How, and L. Breger, *Spacecraft Formation Flying: Dynamics, Control and Navigation*. Elsevier, 2009, vol. 2.

[28] J. Sullivan, S. Grimberg, and S. D'Amico, "Comprehensive survey and assessment of spacecraft relative motion dynamics models," *Journal of Guidance, Control, and Dynamics*, vol. 40, no. 8, pp. 1937–1859, 2017.

[29] H. Curtis, *Chapter 7 - Relative Motion and Rendezvous, Orbital Mechanics for Engineering Students*, 3rd ed. Butterworth-Heinemann, 2013.

[30] C.-T. Chen, *Linear System Theory and Design*. Saunders College Publishing, 1984.

[31] S. W. Shepperd, "Constant covariance in local vertical coordinates for near-circular orbits," *Journal of Guidance, Control, and Dynamics*, vol. 14, no. 6, pp. 1318–1322, 1991.

[32] M. Shibata and A. Ichikawa, "Orbital rendezvous and flyaround based on null controllability with vanishing energy," *Journal of Guidance, Control, and Dynamics*, vol. 30, no. 4, pp. 934–945, 2007.

[33] R. H. Frisbee, "Advanced space propulsion for the 21st century," *Journal of Propulsion and Power*, vol. 19, no. 6, pp. 1129–1154, 2003.

[34] M. J. Turner, *Rocket and Spacecraft Propulsion: Principles, Practice and New Developments*. Springer Science & Business Media, 2008.

[35] M. Martinez-Sanchez and J. E. Pollard, "Spacecraft electric propulsion-an overview," *Journal of Propulsion and Power*, vol. 14, no. 5, pp. 688–699, 1998.

[36] S. Miller, M. L. R. Walker, J. Agolli, and J. Dankanich, "Survey and performance evaluation of small-satellite propulsion technologies," *Journal of Spacecraft and Rockets*, vol. 58, no. 1, pp. 222–231, 2021.

[37] D. M. Goebel and I. Katz, *Fundamentals of Electric Propulsion: Ion and Hall Thrusters*. John Wiley & Sons, 2008.

[38] L. Garrigues and P. Coche, "Electric propulsion: comparisons between different concepts," *Plasma Physics and Controlled Fusion*, vol. 53, no. 12, p. 124011, nov 2011.

[39] S. Mazouffre, "Electric propulsion for satellites and spacecraft: established technologies and novel approaches," *Plasma Sources Science and Technology*, vol. 25, no. 3, apr 2016.

[40] S. Omar and R. Bevilacqua, "Guidance, navigation, and control solutions for spacecraft re-entry point targeting using aerodynamic drag," *Acta Astronautica*, vol. 155, pp. 389–405, 2019.

[41] A. D. Hayes and R. J. Caverly, "Model predictive tracking of spacecraft deorbit trajectories using drag modulation," *Acta Astronautica*, vol. 202, pp. 670–685, 2023.

[42] P. E. Crouch, "Spacecraft Attitude Control and Stabilization: Applications of Geometric Control Theory To Rigid Body Models," *Automatic Control, IEEE Transactions on*, vol. 29, no. 4, pp. 321–331, 1984.

[43] F. L. Markley and J. L. Crassidis, *Fundamentals of Spacecraft Attitude Determination and Control*. New York, NY: Springer, 2014.

[44] M. D. Shuster, "A survey of attitude representations," *The Journal of the Astronautical Sciences*, vol. 41, no. 4, pp. 439–517, 1993.

[45] E. Howell, "Kepler K2 finds first exoplanet, a super-Earth, while surfing Sun's pressure wave for control," *Universe Today*, December 2014.

[46] J. R. Wertz, *Spacecraft Attitude Determination and Control*. Springer Science & Business Media, 2002, vol. 73.

[47] S. Segal and P. Gurfil, "Effect of kinematic rotation-translation coupling on relative spacecraft translational dynamics," *Journal of Guidance, Control, and Dynamics*, vol. 32, no. 3, pp. 1045–1050, 2009.

[48] B. P. Malladi, S. Di Cairano, and A. Weiss, "Nonlinear model predictive control of coupled rotational-translational spacecraft relative motion," in *American Control Conference*, 2019, pp. 3581–3586.

[49] F. Zhang and G. Duan, "Integrated translational and rotational finite-time maneuver of a rigid spacecraft with actuator misalignment," *IET Control Theory & Applications*, vol. 6, no. 9, pp. 1192–1204, 2012.

[50] R. J. Caverly, S. Di Cairano, and A. Weiss, "Electric satellite station keeping, attitude control, and momentum management by MPC," *IEEE Transactions on Control Systems Technology*, vol. 29, no. 4, pp. 1475–1489, 2020.

[51] J. R. Wertz, D. F. Everett, and J. J. Puschell, *Space Mission Engineering: The New SMAD*. Microcosm Press, 2018.

[52] M. S. Murbach, K. M. Boronowsky, J. E. Benton, B. White, and E. Fritzler, "Options for returning payloads from the ISS after the termination of STS flights," in *40th International Conference on Environmental Systems*, 2010, p. 6223.

[53] D. Guglielmo, S. Omar, and R. Bevilacqua, "Drag deorbit device: A new standard reentry actuator for CubeSats," *Journal of Spacecraft and Rockets*, vol. 56, no. 1, pp. 129–145, January-February 2019.

[54] C. L. Leonard, W. M. Hollister, and E. V. Bergmann, "Orbital formationkeeping with differential drag," *Journal of Guidance, Control, and Dynamics*, vol. 12, no. 1, pp. 108–113, January 1989.

[55] J. Virgili, P. C. E. Roberts, and N. C. Hara, "Atmospheric interface reentry point targeting using aerodynamic drag control," *Journal of Guidance, Control, and Dynamics*, vol. 38, no. 3, pp. 403–413, March 2015.

[56] S. Dutta, A. L. Bowes, A. D. Cianciolo, and C. E. Glass, "Guidance scheme for modulation of drag devices to enable return from low Earth orbit," in *AIAA Atmospheric Flight Mechanics Conference*, 2017, p. 0467.

[57] S. R. Omar, R. Bevilacqua, D. Guglielmo, L. Fineberg, J. Treptow, S. Clark, and Y. Johnson, "Spacecraft deorbit point targeting using aerodynamic drag," *Journal of Guidance, Control, and Dynamics*, vol. 40, no. 10, pp. 2646–2652, 2017.

[58] E. Sin, M. Arcak, and A. Packard, "Small satellite constellation separation using linear programming based differential drag commands," in *American Control Conference*, 2018, pp. 4951–4956.

[59] C. Foster, J. Mason, V. Vittaldev, L. Leung, V. Beukelaers, L. Stepan, and R. Zimmerman, "Differential drag control scheme for large constellation of planet satellites and on-orbit results," in *9th International Workshop on Satellite Constellations and Formation Flying*, June 2017, p. 33.

[60] A. Hayes, R. J. Caverly, and D. Gebre-Egziabher, "Atmospheric density estimation in low-earth orbit for drag-modulated spacecraft," in *AAS Guidance, Navigation and Control Conference*, 2022.

[61] J. Picone, A. Hedin, D. P. Drob, and A. Aikin, "NRLMSISE-00 empirical model of the atmosphere: Statistical comparisons and scientific issues," *Journal of Geophysical Research: Space Physics*, vol. 107, no. A12, pp. SIA–15, 2002.

[62] D. C. Woffinden and D. K. Geller, "Observability criteria for angles-only navigation," *IEEE Transactions on Aerospace and Electronic Systems*, vol. 45, no. 3, pp. 1194–1208, 2009.

[63] E. A. Butcher, J. Wang, and T. A. Lovell, "On Kalman filtering and observability in nonlinear sequential relative orbit estimation," *Journal of Guidance, Control, and Dynamics*, vol. 40, no. 9, pp. 2167–2182, 2017.

[64] F. J. Franquiz, J. D. Muñoz, B. Udrea, and M. J. Balas, "Optimal range observability maneuvers of a spacecraft formation using angles-only navigation," *Acta Astronautica*, vol. 153, pp. 337–348, 2018.

[65] K. Black, S. Shankar, D. Fonseka, J. Deutsch, A. Dhir, and M. R. Akella, "Real-time, flight-ready, non-cooperative spacecraft pose estimation using monocular imagery," *arXiv preprint arXiv:2101.09553*, 2021.

[66] B. E. Tweddle and A. Saenz-Otero, "Relative computer vision-based navigation for small inspection spacecraft," *Journal of Guidance, Control, and Dynamics*, vol. 38, no. 5, pp. 969–978, 2015.

[67] N. B. Stastny, "Optimal relative path planning for constrained stochastic space systems," Ph.D. dissertation, Utah State University, 2022.

[68] N. M. Filatov and H. Unbehauen, *Adaptive Dual Control: Theory and Applications*. Springer Science & Business Media, 2004, vol. 302.

[69] A. Hotz and R. E. Skelton, "Covariance control theory," *International Journal of Control*, vol. 46, no. 1, pp. 13–32, 1987.

[70] B. Schutz, B. Tapley, and G. H. Born, *Statistical Orbit Determination*. Elsevier, 2004.

[71] K. S. Narendra and A. M. Annaswamy, *Stable Adaptive Systems*. Courier Corporation, 2012.

[72] A. Weiss, M. Baldwin, R. S. Erwin, and I. Kolmanovsky, "Model predictive control for spacecraft rendezvous and docking: Strategies for handling constraints and case studies," *IEEE Transactions on Control Systems Technology*, vol. 23, no. 4, pp. 1638–1647, 2015.

[73] D. Malyuta, T. Reynolds, M. Szmuk, B. Acikmese, and M. Mesbahi, "Fast trajectory optimization via successive convexification for spacecraft rendezvous with integer constraints," in *AIAA Scitech Forum*, 2020, p. 0616.

[74] G. Boyarko, O. Yakimenko, and M. Romano, "Real-time 6DOF guidance for of spacecraft proximity maneuvering and close approach with a tumbling object," in *AIAA/AAS Astrodynamics Specialist Conference*, 2010, p. 7666.

[75] A. E. Bryson and Y.-C. Ho, *Applied Optimal Control*. New York, NY: Hemisphere, 1975.

[76] J. A. Starek, E. Schmerling, G. D. Maher, B. W. Barbee, and M. Pavone, "Fast, safe, propellant-efficient spacecraft motion planning under Clohessy–Wiltshire–Hill dynamics," *Journal of Guidance, Control, and Dynamics*, vol. 40, no. 2, pp. 418–438, 2017.

[77] L. Breger and J. P. How, "Safe trajectories for autonomous rendezvous of spacecraft," *Journal of Guidance, Control, and Dynamics*, vol. 31, no. 5, pp. 1478–1489, 2008.

[78] D. Aguilar-Marsillach, S. Di Cairano, and A. Weiss, "Abort-safe spacecraft rendezvous on elliptic orbits," *IEEE Transactions on Control Systems Technology*, 2022.

[79] D. A. Marsillach, S. Di Cairano, U. Kalabić, and A. Weiss, "Fail-safe spacecraft rendezvous on near-rectilinear halo orbits," in *American Control Conference*, 2021, pp. 2980–2985.

[80] M. Althoff, C. Le Guernic, and B. H. Krogh, "Reachable set computation for uncertain time-varying linear systems," in *International Conference on Hybrid Systems: Computation and Control*, 2011, pp. 93–102.

[81] A. P. Vinod, A. Weiss, and S. Di Cairano, "Abort-safe spacecraft rendezvous under stochastic actuation and navigation uncertainty," in *IEEE Conference on Decision and Control*, 2021, pp. 6620–6625.

[82] J. B. Rawlings, D. Q. Mayne, and M. M. Diehl, *Model Predictive Control: Theory, Computation, and Design*, 2nd ed. Santa Barbara, CA: Nob Hill Publishing, 2019.

[83] D. Q. Mayne, "Model predictive control: Recent developments and future promise," *Automatica*, vol. 50, no. 12, pp. 2967–2986, 2014.

[84] R. D. Halverson, A. Weiss, and R. Caverly, "A comparison of linear quadratic and nonlinear model predictive control applied to station keeping of satellites in areostationary Mars orbits," in *AIAA SciTech Forum*, 2023, p. 2000.

[85] A. Ansari and D. S. Bernstein, "Satellite drag estimation using retrospective cost input estimation," in *American Control Conference*, 2019, pp. 5804–5809.

[86] S. Hur-Diaz, J. Wirzburger, and D. Smith, "Three axis control of the hubble space telescope using two reaction wheels and magnetic torquer bars for science observations," in *F. Landis Markley Astronautics Symposium*, no. AAS-08-279, 2008.

[87] C. D. Petersen, F. Leve, M. Flynn, and I. Kolmanovsky, "Recovering linear controllability of an underactuated spacecraft by exploiting solar radiation pressure," *Journal of Guidance, Control, and Dynamics*, vol. 39, no. 4, pp. 826–837, 2016.

[88] A. A. Soderlund and S. Phillips, "Autonomous rendezvous and proximity operations of an underactuated spacecraft via switching controls," in *AIAA SciTech Forum*, 2022.

[89] G. R. Frey, C. D. Petersen, F. A. Leve, I. V. Kolmanovsky, and A. R. Girard, "Constrained spacecraft relative motion planning exploiting periodic natural motion trajectories and invariance," *Journal of Guidance, Control, and Dynamics*, vol. 40, no. 12, pp. 3100–3115, 2017.

[90] R. W. Brockett, "Nonlinear systems and nonlinear estimation theory," in *Stochastic Systems: The Mathematics of Filtering and Identification and Applications*, M. Hazewinkel and J. C. Willems, Eds. Dordrecht: Springer Netherlands, 1981, pp. 441–477.

[91] A. Bloch and M. Reyhanoglu, "Controllability and stabilizability properties of a nonholonomic control system," in *IEEE Conference on Decision and Control*, 1990, pp. 1312–1314 vol.3.

[92] A. A. Soderlund, S. Phillips, A. Zaman, and C. D. Petersen, "Autonomous satellite rendezvous and proximity operations via geometric control methods," in *AIAA Scitech Forum*, 2021.

[93] W. J. Harris, "Visual navigation and control for spacecraft proximity operations with unknown targets," Ph.D. dissertation, Air Force Institute of Technology, 2021.

[94] J. Schmidt, D. Geller, and F. Chavez, "Improving angles-only navigation performance by selecting sufficiently accurate accelerometers," Air Force Research Lab Kirtland AFB NM Space Vehicles Directorate, Tech. Rep., 2009.

[95] A. Miller and B. Miller, "Tracking of the UAV trajectory on the basis of bearing-only observations," in *IEEE Conference on Decision and Control*, 2014, pp. 4178–4184.

[96] C.-L. Wang, T.-M. Wang, J.-H. Liang, Y.-C. Zhang, and Y. Zhou, "Bearing-only visual slam for small unmanned aerial vehicles in gps-denied environments," *International Journal of Automation and Computing*, vol. 10, no. 5, pp. 387–396, 2013.

[97] D. Grange, R. Sandhu, A. A. Soderlund, and S. Phillips, "Consensus on region-based pose estimation for satellites," in *IEEE/ION Position, Location and Navigation Symposium (PLANS)*, 2023.

[98] G. N. DeSouza and A. C. Kak, "Vision for mobile robot navigation: A survey," *IEEE Transactions on Pattern Analysis and Machine Intelligence*, vol. 24, no. 2, pp. 237–267, 2002.

[99] C. Kanellakis and G. Nikolakopoulos, "Survey on computer vision for UAVs: Current developments and trends," *Journal of Intelligent & Robotic Systems*, vol. 87, pp. 141–168, 2017.

[100] G. Balamurugan, J. Valarmathi, and V. Naidu, "Survey on UAV navigation in GPS denied environments," in *International Conference on Signal Processing, Communication, Power and Embedded System (SCOPES)*, 2016, pp. 198–204.

[101] A. Bachrach, S. Prentice, R. He, and N. Roy, "Range–robust autonomous navigation in GPS-denied environments," *Journal of Field Robotics*, vol. 28, no. 5, pp. 644–666, 2011.

[102] M. Manteghi, "A navigation and positining system for unmanned underwater vehicles based on a mechanical antenna," in *IEEE International Symposium on Antennas and Propagation & USNC/URSI National Radio Science Meeting*, 2017, pp. 1997–1998.

[103] L. Zhou, X. Cheng, and Y. Zhu, "Terrain aided navigation for autonomous underwater vehicles with coarse maps," *Measurement Science and Technology*, vol. 27, no. 9, p. 095002, 2016.

[104] H. Dong, Q. Hu, and M. R. Akella, "Dual-quaternion-based spacecraft autonomous rendezvous and docking under six-degree-of-freedom motion constraints," *Journal of Guidance, Control, and Dynamics*, vol. 41, no. 5, pp. 1150–1162, 2018.

[105] R. Zappulla, H. Park, J. Virgili-Llop, and M. Romano, "Real-time autonomous spacecraft proximity maneuvers and docking using an adaptive artificial potential field approach," *IEEE Transactions on Control Systems Technology*, vol. 27, no. 6, pp. 2598–2605, 2018.

[106] M. T. Wolf and J. W. Burdick, "Artificial potential functions for highway driving with collision avoidance," in *IEEE International Conference on Robotics and Automation*, 2008, pp. 3731–3736.

[107] Y.-b. Chen, G.-c. Luo, Y.-s. Mei, J.-q. Yu, and X.-l. Su, "UAV path planning using artificial potential field method updated by optimal control theory," *International Journal of Systems Science*, vol. 47, no. 6, pp. 1407–1420, 2016.

[108] A. Weiss, C. Petersen, M. Baldwin, R. S. Erwin, and I. Kolmanovsky, "Safe positively invariant sets for spacecraft obstacle avoidance," *Journal of Guidance, Control, and Dynamics*, vol. 38, no. 4, pp. 720–732, 2014.

[109] A. Weiss, F. Leve, M. Baldwin, J. R. Forbes, and I. Kolmanovsky, "Spacecraft constrained attitude control using positively invariant constraint admissible sets on $\mathrm{SO}(3)\times\mathbb{R}^3$," in *American Control Conference*, 2014, pp. 4955–4960.

[110] C. Danielson, J. Kloeppel, and C. Petersen, "Spacecraft attitude control using the invariant-set motion-planner," *IEEE Control Systems Letters*, vol. 6, pp. 1700–1705, 2021.

[111] R. Okuda, Y. Kajiwara, and K. Terashima, "A survey of technical trend of ADAS and autonomous driving," in *International Symposium on VLSI Design, Automation and Test*, 2014, pp. 1–4.

[112] L. Quan, L. Han, B. Zhou, S. Shen, and F. Gao, "Survey of UAV motion planning," *IET Cyber-systems and Robotics*, vol. 2, no. 1, pp. 14–21, 2020.

[113] A. Weiss, C. Danielson, K. Berntorp, I. Kolmanovsky, and S. Di Cairano, "Motion planning with invariant set trees," in *IEEE Conference on Control Technology and Applications*, 2017, pp. 1625–1630.

[114] K. Berntorp, R. Bai, K. F. Erliksson, C. Danielson, A. Weiss, and S. Di Cairano, "Positive invariant sets for safe integrated vehicle motion planning and control," *IEEE Transactions on Intelligent Vehicles*, vol. 5, no. 1, pp. 112–126, 2019.

[115] C. Danielson, K. Berntorp, A. Weiss, and S. Di Cairano, "Robust motion planning for uncertain systems with disturbances using the invariant-set motion planner," *IEEE Transactions on Automatic Control*, vol. 65, no. 10, pp. 4456–4463, 2020.

[116] C. Danielson, K. Berntorp, S. Di Cairano, and A. Weiss, "Motion-planning for unicycles using the invariant-set motion-planner," in *American Control Conference*, 2020, pp. 1235–1240.

[117] C. Danielson, "Invariant configuration-space bubbles for revolute serial-chain robots," *IEEE Control Systems Letters*, vol. 7, pp. 745–750, 2023.

[118] D. Malyuta, Y. Yu, P. Elango, and B. Açıkmeşe, "Advances in trajectory optimization for space vehicle control," *Annual Reviews in Control*, vol. 52, pp. 282–315, 2021.

[119] D. Malyuta, T. P. Reynolds, M. Szmuk, T. Lew, R. Bonalli, M. Pavone, and B. Açıkmeşe, "Convex optimization for trajectory generation: A tutorial on generating dynamically feasible trajectories reliably and efficiently," *IEEE Control Systems Magazine*, vol. 42, no. 5, pp. 40–113, 2022.

[120] T. A. Johansen and T. I. Fossen, "Control allocation—a survey," *Automatica*, vol. 49, no. 5, pp. 1087–1103, 2013.

[121] S. Phillips, C. Petersen, and R. Fierro, "Spacecraft formation control with intermittent measurement and communication," in *AIAA Scitech Forum*, 2021, p. 1341.

[122] B. P. Malladi, R. G. Sanfelice, E. Butcher, and J. Wang, "Robust hybrid supervisory control for rendezvous and docking of a spacecraft," in *IEEE Conference on Decision and Control*, 2016, pp. 3325–3330.

[123] D. W. Smith and R. Sanfelice, "Autonomous waypoint transitioning and loitering for unmanned aerial vehicles via hybrid control," in *AIAA Guidance, Navigation, and Control Conference*, 2016, p. 2098.

[124] R. G. Sanfelice, *Hybrid feedback control*. Princeton University Press, 2021.

[125] D. Lavell, S. Phillips, and R. G. Sanfelice, "A hybrid PID design for asymptotic stabilization with intermittent measurements," in *IEEE Conference on Decision and Control*, 2018, pp. 737–742.

[126] "Robotic servicing of geosynchronous satellites (RSGS)," https://www.darpa.mil/program/robotic-servicing-of-geosynchronous-satellites.

[127] "Proving satellite servicing," https://nexis.gsfc.nasa.gov/osam-1.html.

[128] C. Blackerby, A. Okamoto, S. Iizuka, Y. Kobayashi, K. Fujimoto, Y. Seto, S. Fujita, T. Iwai, N. Okada, J. Forshaw *et al.*, "The ELSA-d end-of-life debris removal mission: Preparing for launch," in *Proceedings of the International Astronautical Congress, IAC*, vol. 8, 2019.

[129] J. C. Sanchez, F. Gavilan, and R. Vazquez, "Chance-constrained model predictive control for near rectilinear halo orbit spacecraft rendezvous," *Aerospace Science and Technology*, vol. 100, p. 105827, 2020.

[130] G. Bucchioni and M. Innocenti, "Open loop safe trajectory design for cislunar NRHO rendezvous," in *American Control Conference*, 2020, pp. 4337–4342.

[131] R. Nakamura, J. Kikuchi, T. Sasaki, Y. Matsumoto, M. Hidaka, N. Murakami, S. Ueda, and N. Satoh, "Rendezvous trajectory design of logistics resupply missions to the lunar gateway in near-rectilinear halo orbit," *Journal of Space Safety Engineering*, 2023.

[132] A. Colagrossi, V. Pesce, L. Bucci, F. Colombi, and M. Lavagna, "Guidance, navigation and control for 6DOF rendezvous in cislunar multi-body environment," *Aerospace Science and Technology*, vol. 114, p. 106751, 2021.

[133] J. A. Christian and E. G. Lightsey, "Review of options for autonomous cislunar navigation," *Journal of Spacecraft and Rockets*, vol. 46, no. 5, pp. 1023–1036, 2009.

[134] P. Elango, S. Di Cairano, K. Berntorp, and A. Weiss, "Sequential linearization-based station keeping with optical navigation for NRHO," in *AAS/AIAA Astrodynamics Specialist Conference*, 2022.

[135] M. Hapgood, H. Liu, and N. Lugaz, "SpaceX—sailing close to the space weather?" *Space Weather*, vol. 20, no. 3, p. e2022SW003074, 2022.